Available online at www.sciencedirect.com

jmr&t Journal of Materials Research and Technology

journal homepage: www.elsevier.com/locate/jmrt

Effect of graphene oxide as a nanomaterial on the bond behaviour of engineered cementitious composites by applying RSM modelling and optimization

Naraindas Bheel [a,*], *Bashar S. Mohammed* [a], *Montasir Osman Ahmed Ali* [a], *Nasir Shafiq* [a], *Dorin Radu* [b]

[a] *Department of Civil and Environmental Engineering, Universiti Teknologi Petronas, Bandar Seri Iskandar, Tronoh, Perak, 32610, Malaysia*

[b] *Faculty of Civil Engineering, Transilvania University of Brașov, Turnului Street 5, Brașov, 500156, Romania*

ARTICLE INFO

Article history:
Received 28 April 2023
Accepted 31 July 2023
Available online 6 August 2023

Keywords:
Graphene oxide
ECC
Pull-out test
Bond
Response surface methodology
Multi-variate optimization

ABSTRACT

A crucial aspect of the design approach for bar-reinforced concrete buildings is the proper transfer of loads between the concrete and steel reinforcement via bonding. Bar pull-out tests were done to see how graphene oxide (GO) affected the bond strength, bond energy, and bond stress–slip response of deformed reinforcing bars implanted in engineered cementitious composites (ECC). This was done to improve the bond strength of steel/concrete composites. This article examines the bonding behaviour of steel reinforcing bars in a mixture of GO-modified ECC. The findings of pull-out assessments conducted on two distinct diameters (12 and 16 mm) of reinforcement steel bar inserted in ECC are initially provided. The investigation's findings are then utilised to determine the bond-slip interactions that describes the relations between the ECC mixtures and steel reinforcement bars. According to the experiment results, the introduction of GO as a nano-reinforcement in the ECC mixture had a considerable positive effect on the bar-matrix interactions owing to its bridging function. After 28 days, the bond strength of steel bars with widths of 12 and 16 mm was increased by 54.80% and 26.70%, respectively, when 0.05 wt% of GO was added to 1% of PVA fibre. The response surface methodology (RSM) is employed for developing predictive algorithms, which are then utilised in performing multi-variate optimization on bond-slip parameters, including bond strength, bond slip and bond energy. The acquired actual and predicted findings suggest that the created models are adequate for interpreting the bond performance of reinforcement steel bars in the GO-ECC.

* Corresponding author.
E-mail address: naraindas04@gmail.com (N. Bheel).

https://doi.org/10.1016/j.jmrt.2023.07.278

1. Introduction

In the past couple of decades, scientists have intensified their efforts to produce high-performance fibre-reinforced cementitious composites (HPFRCC) as a result of their desire to enhance structural performance. The various kinds of fibres, binders, aggregates, additives, and chemical additives have been utilised to generate a variety of HPFRCC products [1,2]. Engineered cementitious composites (ECC) is the form of HPFRCC product and it is created using micromechanics concepts. By modifying the behaviour of the fibre, cementitious mixtures, and fibre-mixtures interconnect, ECC may create strain-hardening and multiple fracturing properties underneath uniaxial stress. Typically, the ECC utilises 2% or less of fibre by volume fraction to achieve these characteristics. Prior to the appearance of softening [1,3,4], the multiple cracking qualities produced commence a pseudo-strain hardening characteristics that may obtain strains between 3 and 8%, which is about 300 and 800 times that of conventional concrete. The compressive strength ranges from 35 to 100 MPa, whereas the usual tensile strength ranges from 2 to 7 MPa [1,3–5]. Due to their superior mechanical qualities, ECC composites have been researched for a variety of structural design, restoration, and retrofit purposes [6–8] in an effort to reduce deterioration, improve elastic properties, and enhance performance beneath extreme loading situations. The enhanced mechanical characteristics of ECC components may result in increased load and shear capacity, impact resistance, fracture toughness, and energy absorption [8,9]. This will improve the safety, durability, efficiency of development, and long-term growth of infrastructure facilities. Similarly, slabs and beams built using ECC materials exhibit enhanced flexural toughness, superior ductility, and energy absorption [3,5,10]. The increased characteristics of ECC materials may reduce the reinforcing demands of structural components for both flexure and shear [11,12]. However, some degree of reinforcement is required to achieve sufficient strength. The propagation of bond stresses in ECC results in the combined interaction between the reinforcement steel and ECC. The bond quality of reinforcement structures has an impact on designing the structural elements, particularly in the context of development dimension, anchorage, and splice requirements [13]. In the same way, the ability of a fibre mix bond to transmit stress throughout the fibre content-matrix stages also governs the utilisation of disintegrating fibres to enhance the toughened assets of mixes [14]. In contrast to Portland cement (PC) and high-volume fly ash, a variety of ingredients have been used to generate ECC mixes. The substitutions for cement components like metakaolin, ground granulated blast furnace (GGBFS), silica fume, fly ash, millet husk ash, wheat straw ash, nano silica (NS), and nano-TiO2 have been used for partial or whole substitution [4,15,16]. The majority of the alternative materials have been included to either reduce manufacturing costs or enhance the performance of ECC components in construction. There has been minimal study on strengthening the steel matrix bond in nanomaterial-modified ECCs, particularly graphene oxide (GO)-modified ECCs, despite the fact that several uses of ECC substances have been proposed.

GO is regarded as among the most beneficial graphene derivatives for cementitious mixtures due to its durable attachment with a variety of oxygen-functional groups [17]. Due to the presence of reactive hydroxyl groups in GO, composites diffuse efficiently [18]. It works well as an activator, but it is brittle and expensive to use graphene in cement products. Previous studies [19] showed that the bending/compressive forces of mixtures blended with GO were much higher than those of control mixture. This is due to the recognition that GO boosts the ECC's toughness through a beneficial activation procedure, restricting the initiation and spread of crack formation, improving transport properties, and raising the sensitivity of the freezing and tanning processes [18]. In addition, the total porosity of cementitious composites incorporating 1% GO decreased from 25.21% to 10.61% [20]. The goal of GO is to help improve the final product's concentration of calcium silica hydrate (C–S–H), decrease the porousness of the microstructure, and stabilise the composite components [21]. As compared to ordinary fibres, the addition of GO improves nanoscale productivity owing to the enhanced specific surface area and more availability of functional groups [22]. As a consequence, it delivers nanoscale performance that is notably better than that of its competitors. The addition of GO enhances the reactivity of PC hydration products and stimulates the building of covalent bonds [23]. Consequently, it improves the structural interface and productivity of PC-based mixtures [18].

GO is utilised to growth the hydration of cement, resulting in more stable and durable concrete [24]. The oxygenation functions of GO contribute to it being a highly soluble cementitious matrix-reinforcing component in contrast to numerous carbon-based nanomaterials, which agglomerate rapidly in cementitious matrix [25]. Prior studies indicate that the introduction of GO accelerates the PC hydration in matrix. This may be attributable to the oxygenation functional groups affixed to GO nanosheets' shape, which renders them readily available to PC components, thereby improving the cement-water relationship by serving as nuclei for cement stages [26]. GO, like graphite nanoparticles, seems to be a promising nanoparticle for enhancing the characteristics of cement-based composites [23].

The design of experiment method known as the response surface methodology (RSM) procedure is used to investigate the impact and interactions between various components of the variable associated with the response. The main objective is to streamline the testing process and improve the findings, much like the traditional Taguchi method. The RSM technique, according to Bradley et al. [27], involves evaluating the response surface shape as well as the closest maximum (+1), minimum (−1) and ridges approach in order to pinpoint the ideal response spot. To create a response surface that defines the optimal values for the response factor, the RSM approach assesses the combined effect of the first order, second order, and combination effects amongst the elements. The RSM method, like other experimental design approaches, uses a mathematical method to resolve an issue, lowering the quantity of laboratory experiments as well as the cost and length of the study. In order to increase the model's accuracy and reliability, it also assesses how each element interacts with the others. Nonetheless, the quadratic order to which the empirical findings correlate may not accurately represent all curved structures [28]. RSM provides a comprehensive analysis tool for findings and discoveries, but it is unable to govern how data is collected. There are other ways to

gather data besides using the orthogonal Array, like the Taguchi technique. A number of approaches are used, including the Box-Behnken design (BBD), the central composite design (CCD), and three levels (3 k) of complete designs with factorial elements. Poor information gathering and performance outcomes result from the need for more tests as the variety of levels rises [29]. As a result, in comparison to RSM, its applicability is rather restricted. Numerous studies [30] have looked at the effectiveness of the latter three techniques. The past 10 years have seen an increase in the use of optimal experimental designs compared to conventional methods. This is because they are more flexible and able to handle a wider range of problems than conventional designs [26]. RSM, which includes research designs, combination proportioning, building numerical models, and combination optimization, was performed using design expert software. In this study, GO and polyvinyl alcohol (PVA) fibre are used as independent variables in order to examine their effects on the bonding behaviors of ECC.

In this study work, the bonding ability of steel reinforcing embedded in GO-ECC is studied. Pull-out samples are frequently utilised for evaluating the features of a bond because they are easy to make and easy to evaluate [23,24]. However, because of the stress fields, specimens subjected to pull-out tests are the least representative and hence do not accurately model a bond situation in actual structure [25]. Still, a number of the problems with the pull-out examination could be fixed by making changes to the equipment used to test the samples. This is done to reduce the influence of the compressive stress on the steel rod surface throughout the compression test [23]. In spite of their shortcomings, pull-out tests provide a simple and inexpensive method for comparing bond behaviour with regard to concrete forms, cover, rebar dimensions [23], types of fibres, and fibre volume [26]. Pull-out testing was utilised to analyse the pull-out loads, failure mechanisms, and bonding stress of GO-ECC samples. The examinations were carried out for the reasons listed below: (i) to examine the influence of GO in ECC ingredient on bonding stress of reinforcement steel rod, (ii) to measure the impact of reinforcement diameter and cover on the reinforcing steel rod, and (iii) to assess the composite contributions of various fibre volumes and GO quantity in ECC materials. In addition, a RSM mathematical model is provided, and multi-objective optimization solution characteristics are established and experimentally confirmed.

2. Research significance

The application of GO in ECC for assessing bond strength, bond energy, and bond slip is of great scientific significance due to its potential to revolutionise the area of building materials. The extraordinary mechanical and chemical characteristics of GO, a two-dimensional (2D) nanomaterial generated from graphene, might improve the performance of cementitious composites. To begin, examining the bond strength between GO and cementitious matrices can provide useful information regarding the material's capacity to enhance ECC adhesion qualities. Conventional cementitious composites often have poor interfacial bonding, resulting in decreased durability and structural integrity. Experts may examine the augmentation in bond strength, which can lead to enhanced load transmission, fracture resistance, and overall mechanical strength of ECC structures, by introducing graphene oxide.

Secondly, evaluating the bond energy in GO-modified ECC (GO-ECC) can provide useful information regarding the energy required to break the interfacial bonds between the nanomaterial and the cementitious matrix. Understanding the bond energy is crucial for predicting the composite material's performance under various loading conditions and identifying potential failure mechanisms. In addition, it can help optimize the concentration and distribution of GO to accomplish the desired bond energy, harmonising the strength and ductility of the material. Finally, Examining the bond slip characteristics of GO-ECC can reveal its ability to endure deformation and prevent slippage between reinforcing fibres and the cementitious matrix. This makes it ideal for increased structural performance, including seismic-resistant constructions, by identifying the material's ability to avoid debonding and improve fracture resistance.

The importance of this study is seen in the possible advantages that GO-ECC may provide for the building sector. ECC structures may display better mechanical qualities, higher durability, and improved resistance to environmental degradation by enhancing the bond strength, bond energy, and bond slip characteristics. As a result, less maintenance and repair work may be required as infrastructure becomes more durable and sustainable. Furthermore, by comprehending the basic principles behind the bond strength, binding energy, and bond slip in GO-ECC, it will be possible to improve the composition of the material, its production methods, and its application strategies. This information may be used to direct the design and engineering of sophisticated cementitious composites, facilitating the creation of cutting-edge building materials with higher performance and a variety of uses. In conclusion, research into the usage of GO in ECC for figuring out bonds' strengths, energies, and slips is important since it might progress the development of construction materials. The results of this study have the potential to solve the problems facing the construction industry and advance materials science and engineering by enabling the

Table 1 – XRF of PC and FA.

Materials	Compound (%)									Specific Gravity	Blaine fineness (cm^2/g)	Loss on ignition
	SiO_2	Al_2O_3	Fe_2O_3	MnO	CaO	MgO	Na_2O	K_2O	T_2O			
FA	57.01	20.96	4.15	0.033	9.79	1.75	2.23	1.53	0.68	2.38	2900	1.25
Cement	20.76	5.54	3.35	–	61.4	2.48	0.19	0.78	–	3.15	3250	2.20

Table 2 – Properties of polyvinyl alcohol fibre.

Type	Grade	Length	Diameter	Aspect Ratio (l/d)	Tensile Strength	Modulus of Elasticity	Specific Gravity
PVA	REC S-15	12 mm	40 μm	462	1600 MPa	41 GPa	1.3

creation of infrastructure that is more robust, long-lasting, and sustainable.

3. Experimental program

3.1. Materials

In this research, PC is used as a binding agent, which is in line with ASTM C150 [31]. Though, Class F fly ash (FA) that satisfies ASTM C618 [32] requirements is applied in this investigational determination, Table 1 lists the X-ray fluorescence (XRF) and physical characteristics of PC and FA. However, GO is employed in varying amounts as a nanomaterial in the ECC combination. The sand is used as fine aggregates that pass through a No. 4 screen. In addition, the PVA fibre created by Kuraray Japan is used as a fibre in this experimental effort. The fibre surface was treated using 1.2% oil by weight to adjust the fibre content/matrix interaction characteristics. Table 2 lists the qualities of the fibre. The superplasticizer is applied as chemical admixture in the ECC and it is utilised in various amounts within the ECC combination. In addition, the potable water is used for the purpose of mixing and curing this scientific investigation.

3.2. Mixture proportions of ECC

To achieve the objective of this research, the RSM method was used, and the two independent variables (input factors) tested were GO and PVA at three levels: 0.05, 0.065, and 0.08% of GO by cement weight and 1%, 1.5%, and 2% of PVA fibre by volume fraction, correspondingly. However, the FA-to-cement ratio, water-to-binder ratio, and sand-to-binder ratio for all ECC mixes were 1.20, 0.30, and 0.36, respectively; obviously, it depends on the proportions for the most extensively utilised ECC in the majority of research (ECC-M45) [33,34] and a plasticizer of 1% by weight of PC was used in this experiment. In addition, the thirteen experimental runs were produced using the RSM CCD approach. As shown in Table 3, the mixes included several combinations and concentrations of the input variables, as well as five random repeats of each parameter. The goal of the duplicate mixes was to verify the experiment's validity and safeguard against any variances. In addition, the RSM evaluates the effect of input element relationships on answers. As reactions developed, bond strength, bond energy, and bond slip were explored.

3.3. Testing procedure for pull-out test setup

The cubical samples (50 mm × 50 mm x 50 mm) were cast and tested for compressive strength by obeying the BS EN 12390-3 [35] standards as shown in Fig. 1 (a). Similar to this, the Japanese Society of Civil Engineers (JSCE) protocol was followed to test the tensile strength of dog-bone-shaped specimens (420 mm × 120 mm x 30 mm) made with GO-ECC combined with various concentrations of PVA fibre as shown in Fig. 1 (b) [36]. However, Pull-out testing was done using cylindrical samples (200 mm × 100 mm) and concentrically positioned steel bars as shown in Fig. 1 (c). The investigational program examined the impact of various factors on the bonding between GO-ECC mixes and implanted steel bar reinforcement. Throughout the fabrication of the samples, attention was paid to guarantee that the quantity of deformations (ribs) is the similar for each diameter and length of implanted reinforcement. With a tolerance of 0.5 ribs, the total quantity of deformations (ribs) introduced into every sample depending on the dimension of a reinforcement was kept the same [37]. As seen in Fig. 1(c), samples made of GO-ECC for pull-out testing

Table 3 – Mix proportion of GO-ECC generated by RSM.

Mix ID	Ingredients (%)		Number of Constituents used in ECC (kg/m^3)			
	GO	PVA	PC	Fly Ash	Sand	Water
M0	0.00	2	583	700	467	385
M1	0.05	1.5	583	700	467	385
M2	0.065	2	583	700	467	385
M3	0.065	1.5	583	700	467	385
M4	0.08	1.5	583	700	467	385
M5	0.065	1.5	583	700	467	385
M6	0.065	1	583	700	467	385
M7	0.05	2	583	700	467	385
M8	0.065	1.5	583	700	467	385
M9	0.05	1	583	700	467	385
M10	0.065	1.5	583	700	467	385
M11	0.08	1	583	700	467	385
M12	0.065	1.5	583	700	467	385
M13	0.08	2	583	700	467	385

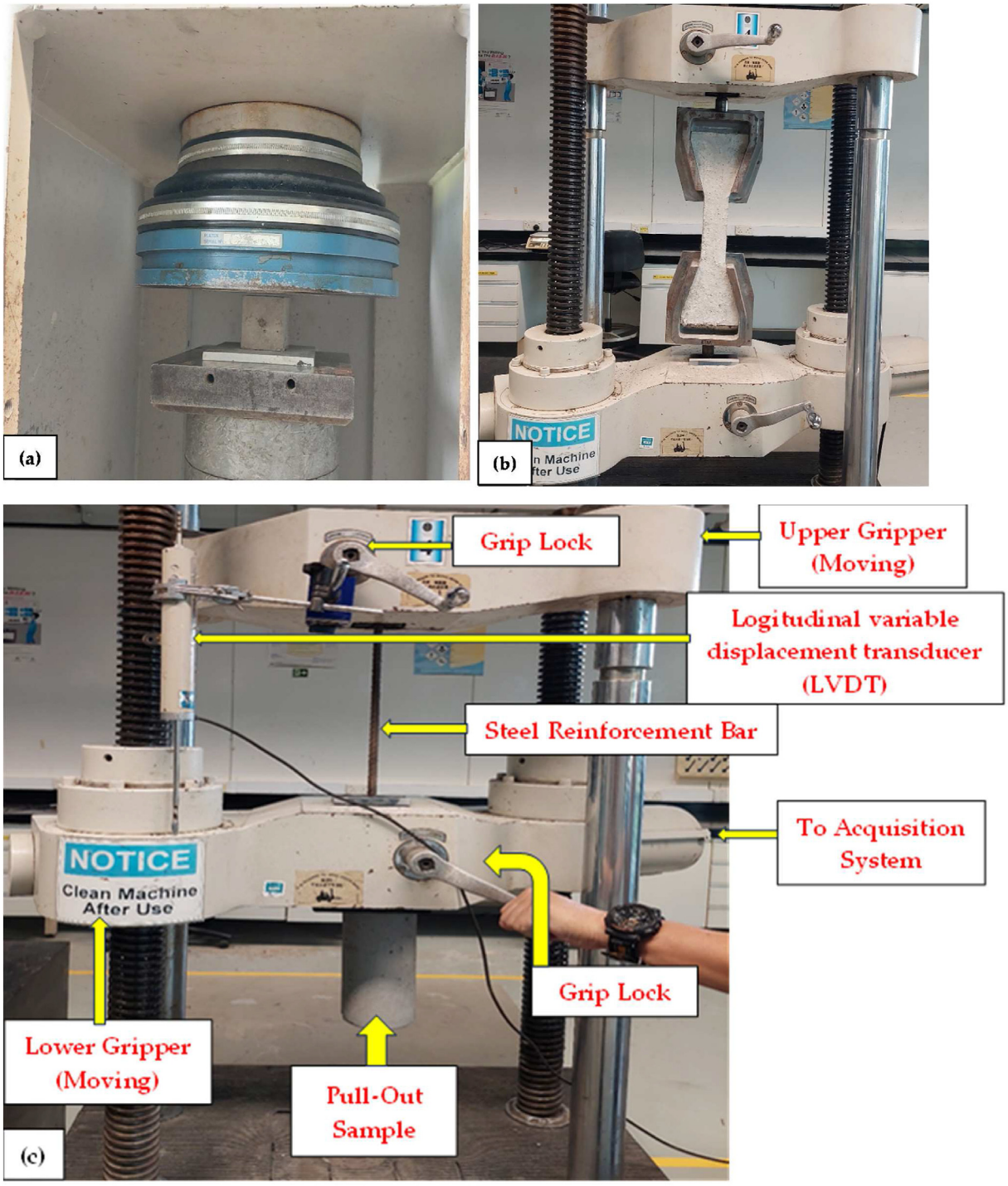

Fig. 1 – Experimental testing setups for (a) Compressive strength, (b) Tensile strength and (c) Pull out Testing.

were constructed in cylindrical moulds with reinforcing bars (d = 12 and 16 mm) placed in the centre of the mould. The bonding length at the mid-embedded length was established at 9 times the bar diameter for each diameter size of reinforcing bar (9 d). This was done to achieve a consistent spreading of bonding stress and to prevent steel bars from yielding under the maximum pull-out force [38,39]. The debonding length for every reinforcement rod was isolated at both edges of the implantation length by applying a flexible plastic hose with a dimension similar to dimension of steel rod. A silicone type of sealant was used to prevent substantial ECC from entering the debonded length at each end of the hose covered. In order to implement monotonic direct tensile forces, the specimens shown in Fig. 1(c) were fastened to a 1000-kN-capacity electro hydraulically controlled testing actuator. The actuator was equipped with a load cell to monitor the load that was placed by means of an internal amplification system attached to the controller. The

information was obtained from coupled information gathering system and controller input network. The assessment was carried out with controlled displacement. An actuator with a built-in linear variable differential transducer (LVDT) and an outer linear potential differential transducer (LPDT) were used to measure the displacement at the loaded end on UTM. On the other hand, a separate external LPDT was used to measure the displacement at the unloaded end. To allow sufficient time to catch variations throughout the test, the displacement frequency was kept at 0.010 mm per second. The bond slip is the relative difference between a steel reinforcement rod and an ECC cylinder sample. Bond slip is a difference between LVDT assessments and the steel reinforcement rod's elongation on the outside of the ECC sample. Therefore, the greatest recorded slip, which causes a significant pull-out force, accurately reflects the highest local bonding slip at midway point of the implanted length of the steel rod [38]. Because the bond length is very small in comparison to the specimen size and is located in the centre of the embedded length of the steel rod, it is appropriate to assume that the stress distribution remains constant throughout the investigated bond length [38]. The goal of the assessment was to evaluate the distribution of bonding stress and the associated bond slip displacement during testing time. Bonding strength is defined by the maximum bonding stress in the bonding stress-slip curve, whereas bond energy is estimated as the area underneath the bond stress-slip curve [38].

4. Results and discussions

4.1. *Compressive strength of GO-ECC*

Fig. 2 indicates the outcome of compressive strength were performed ECC samples introducing the several content of GO as nanoparticle along with various percentages of PVA fibre after 28 days. The maximum compressive strength was observed by 78.60 MPa at 0.05% of GO as nanoparticle along with 1% of PVA fibre while the minimum strength was calculated by 58.40 MPa at 0.08% of GO as nanomaterial reinforced with 1% of PVA fibre at 28 days respectively. Similarly, the highest outcome of compressive strength was recorded at 0.05% GO and minimum strength was noted at 0.08% of GO accumulation with 1.5% and 2% of PVA fibre in ECC at 28 days consistently. Finding has been indicated that the usage of 0.05% GO as nanoparticles provides optimum outcome as compared to other all mixtures of ECC and further inclusion of GO in ECC, the strength gets reduce. This enhancement in the compressive strength is ascribed to the GO as nanoparticle which seals the voids of ECC [40,41]. Moreover, it is attributable to the accumulation of nanoparticle sizes of GO that occupy the voids left by the remaining ECC ingredients [40,41]. In addition, the intense interface interaction between GO and mortar in a matrix, requiring physical linking and chemical interaction, influences the mechanical characteristics of reinforced composites. GO's convex edges improve its mechanical interaction with the cementitious binder. The development of covalent connections is a consequence of chemical reactions between oxygen functional groups and products of hydration [42]. According to research by Yang et al. [43] and Lu et al. [44], GO serves as an establishment site for the cement hydration. The presence of functional groups found on GO basal surfaces might significantly increase the interfacial binding between them and Ca^{2+} ions derived from C–S–H, according to molecular mechanics studies. Because of the stronger link between the GO and PC matrix, stress may travel from one area to another more easily, enhancing the compressive strength [45]. The incorporation of greater than 0.05% GO nanomaterial in the ECC mixture reduces its compressive strength after each curing time. The decline is a

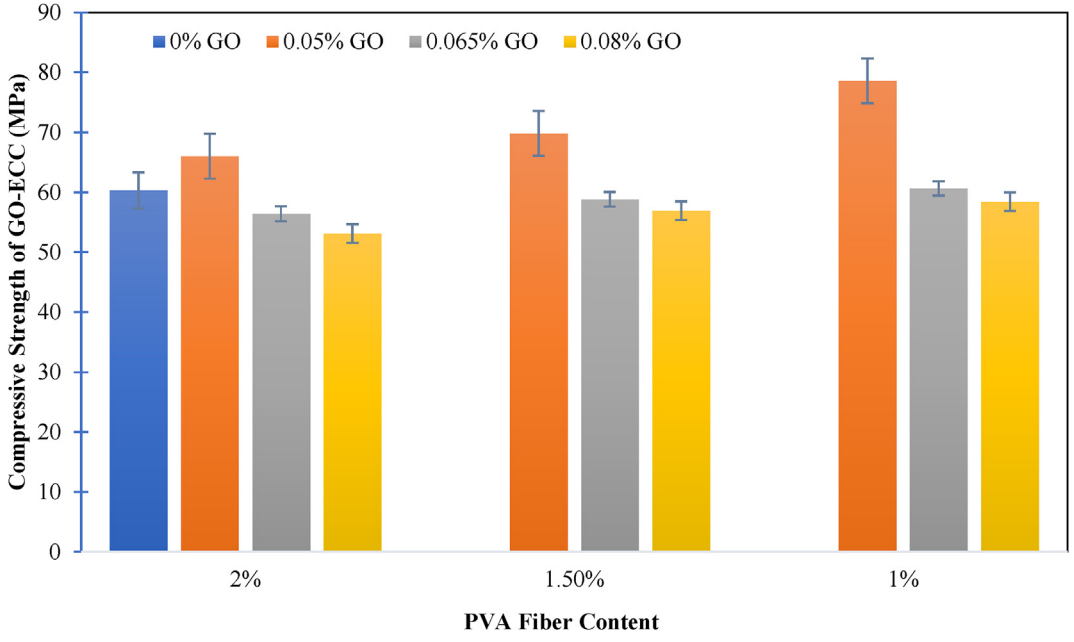

Fig. 2 – Compressive strength of GO-ECC mixture.

result of a higher percentage of GO agglomerates, which weakens the interfacial connection between GO particles and cement hydration [46]. In contrast, this decrease in strength is attributed to the detrimental effect of greater quantities of GO, which causes dispersion problems of GO in the mixture of cement, thereby delaying the suitable use of GO to improve the mechanical properties of the cement matrix [47]. Several investigations have determined that thoroughly mixed GO nanomaterials are much less effective than well-dispersed GO sheets in enhancing the mechanical characteristics of the mortar matrix due to their more substantial surface area utilisation in accelerating the process of hydrating through nucleic action [48]. Moreover, the decrease in compressive strength of the ECC combination is caused by the addition of additional PVA fibre reinforcement, which results in a stiffer mixture with more spaces, both of which reduce compressive strength. On the other hand, the weak spots in the combination where there is an inadequate quantity of cement paste are caused by the clumping effect of fibre, which causes the strength to decrease with higher fibre concentration. These results are comparable to those stated by Wang et al. [26] and Kang et al. [49].

4.2. *Direct tensile strength of GO-ECC*

Fig. 3 depicts the tensile strength at 28 days of an ECC combination including varying concentrations of GO as nanoparticles and 1%, 1.5%, and 2% PVA fibre. At 28 days, the maximum tensile strength is 5.80 MPa at 0.05% GO, whereas the lowest tensile strength is 4.60 MPa at 0.08% GO particles in ECC combined with 1% PVA fiber. In a similar way, after 28 days, the highest tensile strength of ECC containing 1.5% PVA fiber is 5.60 MPa at 0.05% GO, and the smallest tensile strength of ECC added with 1.5% PVA fiber is 4.20 MPa at 0.08% GO particle. It has been determined that the tensile strength of ECC containing 1.5% PVA fiber and different concentrations of GO is higher at 1% PVA and multiple concentrations of GO. Furthermore, the greatest tensile strength is projected to be 5.50 MPa at 0.05% GO, whereas the smallest amount of tensile strength is reached at 4.0 MPa at 0.08% GO particle in ECC mixed with 2% PVA fiber on 28 days. According to the study's findings, the tensile strength decreases as the quantity of PVA fibre in the ECC increases. This decrease in tensile strength is caused by increased air spaces and porosity as a consequence of inadequate compaction of a large amount of PVA fibre in the ECC. Moreover, the tensile strength is seen to be greatest at 0.05% GO particle in the ECC, with additional incorporation of GO in the ECC causing the tensile strength to drop. The fineness of nanoscale particles of GO in comparison to the remaining ingredients in ECC replaces the voids left by the remaining elements of the ECC up to 0.05%, resulting in an increase in the ECC inter-transition zone [41,43,50–54]. On the Other hand, the improvement in strength is associated to the bridging effect of GO particle to certain limit in ECC [53,55–59]. The incorporation of 0.05% GO into the ECC reduces the strength owing to GO agglomerate; it is difficult to attain homogeneous dispersion of GO within the cement matrix, which may be caused by GO sliding over one another [53,54].

4.3. *Pull out loads of GO-ECC*

The findings of pull-out tests conducted on 12-mm and 16-mm reinforcement bars made of steel imbedded in a cylindrical sample after 28 days of curing are depicted in Figs. 4 and 5, respectively. A comprehensive investigation of pull-out experiment outcomes reveals that the pull-out load in ECC samples integrated with GO developed during the study period augmented as the quantity of GO components, PVA filaments,

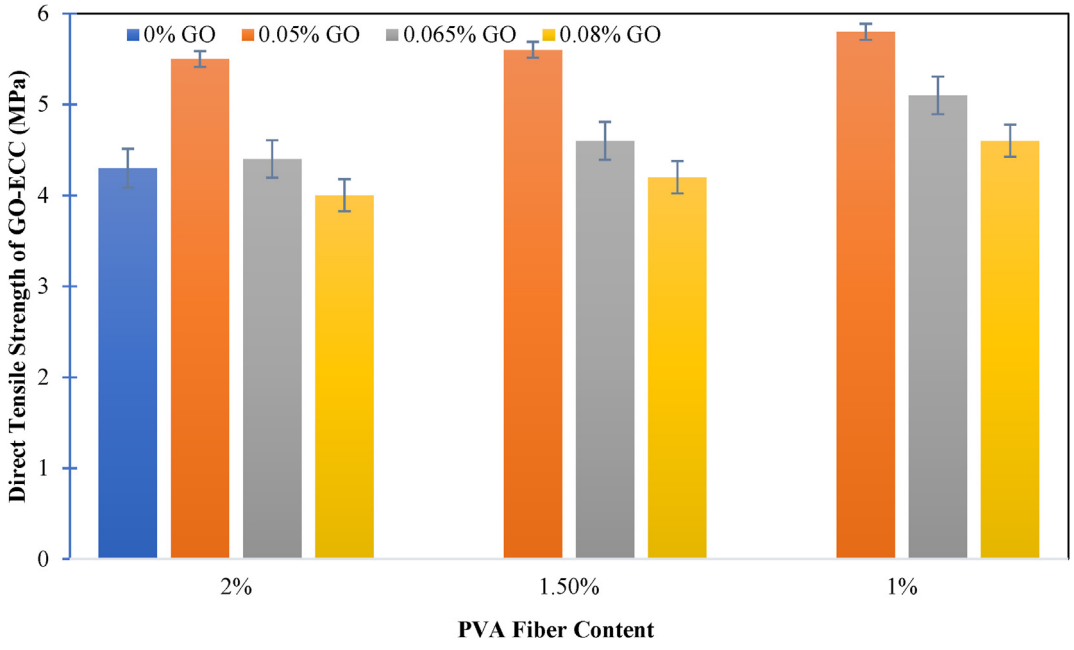

Fig. 3 – Direct tensile strength of GO-ECC Mixture.

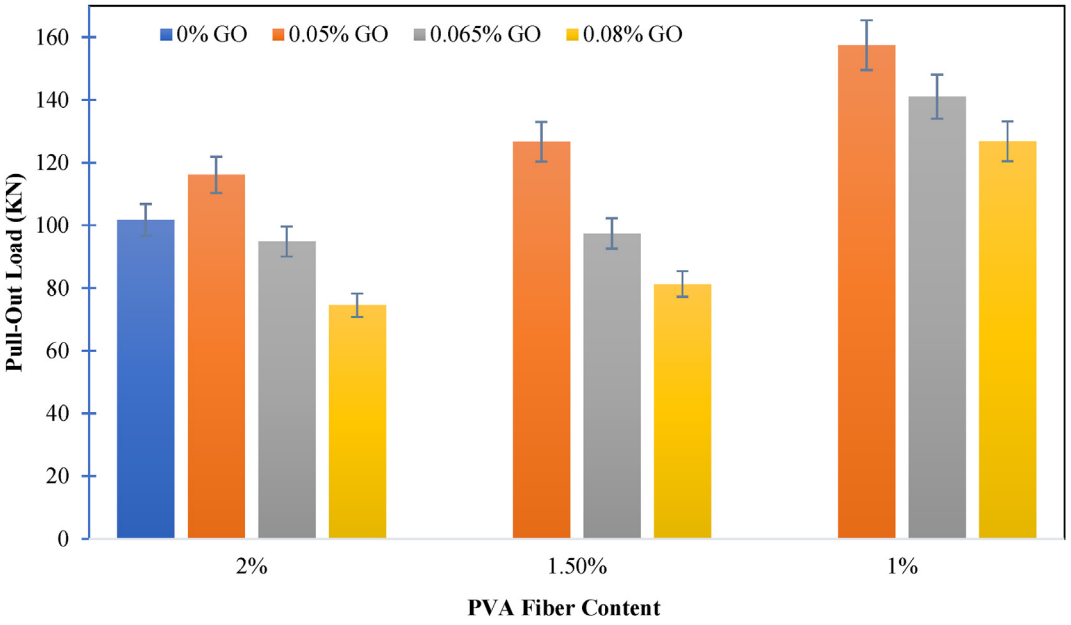

Fig. 4 – Pull out load of GO-ECC of 12 mm diameter steel bar.

and steel bar diameter increased. After 28 days, it showed that the incorporation of 0.05% GO and 1%, 1.5%, and 2% of PVA fibre in 12 mm diameter of steel reinforcement rod increased pull-out force by approximately 54.80%, 24.50%, and 14.16% in comparison with the control ECC compositions respectively. However, the minimum pull-out load of ECC accumulation with 1.5% and 2% of PVA fibre was recorded by 20% and 26.77% at 0.08% of GO particles of 12 mm reinforcement steel bar for 28 days correspondingly. Similarly, after 28 days, the combination containing 1%, 1.5%, and 2% PVA fibres and 0.05% GO particles increased pull-out loads in 16-mm diameter reinforcement steel rods by 26.70%, 11.86%, and 9.95% when compared to the control mix. Moreover, the pull-out load of ECC accumulation with 1.5% and 2% of PVA fibre was recorded by 10.70% and 19.36% at 0.08% of GO particles which is lower than that of control mixture of 12 mm reinforcement steel bar for 28 days correspondingly. These findings demonstrated that the pull-out load of GO-ECC steel reinforcement bonds

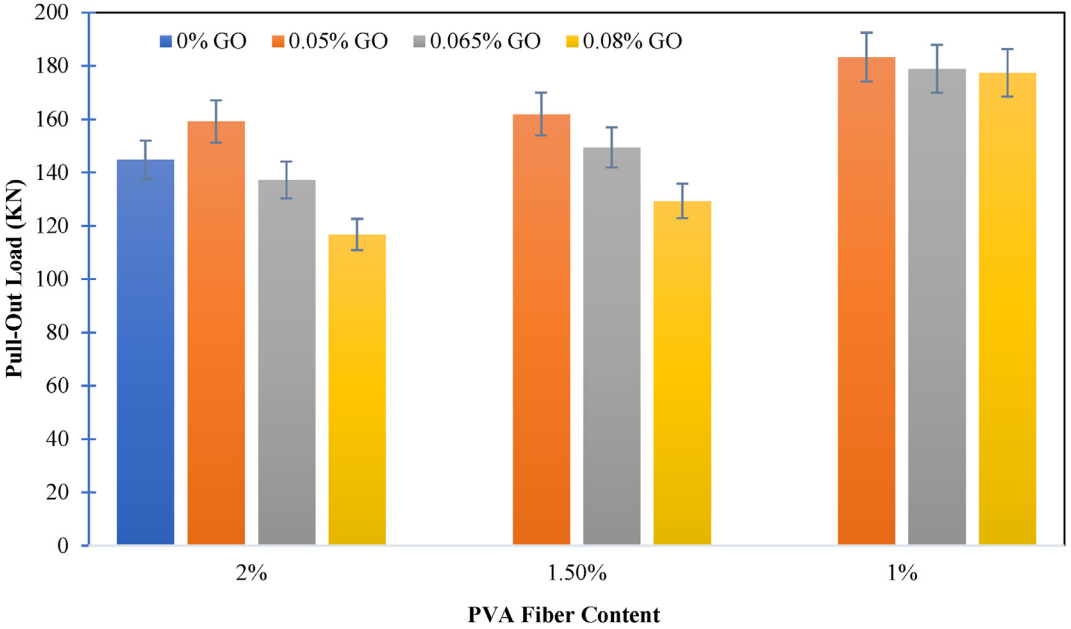

Fig. 5 – Pull out load of GO-ECC of 16 mm diameter steel bar.

increased for diameters of 12 mm and 16 mm when compared to other GO-ECC mixes mixed with 1.5% and 2% PVA fibre. Investigations in scientific literature have demonstrated that integrating GO and PVA fibres tends to strengthen the bonding between PC mixture and reinforcement steel rod, which is consistent with the findings of our research. In a comparable work, Lee et al. [39] used PVA fibre to create an ECC mix that, in comparison to regular concrete, had a greater binding tension between the steel reinforcement and the ECC matrix. The strain-hardening tendency brought on by the connection between the fibre and matrix led to greater bond stress. According to research by Noushini et al. [60], adding 0.25% PVA fibres to PVA fibre reinforced concrete boosted its 28-day compressive strength by 11.6% and 7.5%, correspondingly. The interplay of the fibre-matrix and the PVA fibres' capacity to bridge cracks is what leads to the increase in compressive strength. The addition of nanomaterials to PVA fibre mixtures increases packing density throughout the interfacial transition zone (ITZ) and PC mixture [61,62]. The packing density and toughness of the ITZ connecting PVA fibre as well as PC mix affect interfacial resistance [62,63]. According to published research, nanoparticles enhance ITZ characteristics, which correspond to an increase in bond strength rather than a chemical bond [64,65]. As depicted in Figs. 4 and 5, an increase in bond strength enhances the composite's pull-out load and bonding stress. In the same way, Table 4 displayed the bond energy which increases with the enhancement of ITZ between the reinforcement steel rod and PC mixture and PVA filaments and PC mixture [62]. This may be attributed to the higher bonding strength at the ITZs of reinforcement steel rod and PVA filaments as a result of a stronger composite [62]. Moreover, this reduction in pull-out force of the ECC combination is caused by the accumulation of additional PVA fibre reinforcement, which results in a stiffer mixture with more spaces, which cause reduction in pull-out force. In addition, the weak spots in the combination where there is an inadequate quantity of cement paste are caused by the clumping effect of fibre, which causes the pull-out load/bond strength to decrease with higher fibre concentration.

4.4. *Influence of steel bar on the maximum pull-out loads*

After analysing the pull-out assessment findings given in Figs. 4 and 5 and Table 4, it became clear that a greater force was required as the diameter of the deformed steel reinforcement bars rose to remove them from the composite material. For mix 9 in Table 4, it is found that the ultimate pull-out force was noted by 157.5 KN when the diameter of the deformed reinforced steel bar is 12 mm and by 183.30 KN when it is increased from 12 to 16-mm. Improvements are seen for various mixes as the diameter grows. The rise in pull-out load with increasing rod diameter is a result of the dimensional characteristics of the steel bar segments growing with increasing bar diameter [65].

4.5. *Bond strength of GO-ECC*

Figs. 6 and 7 show the bond strength measured using pull-out tests of reinforcement bars made of steel with diameters of 12-mm and 16-mm at 28 days for all mixes of ECC combined with varying amounts of GO as nanoparticles and 1%–2% PVA fibres. The optimum bond strength of ECC blended with 1% of PVA fibre is recorded by 38.70 MPa at 0.05% of GO particle of 12 mm diameter of reinforcement steel bar while the minimum bond strength of ECC accumulation with 1% of PVA fibre is estimated by 31.14 MPa at 0.08% of GO particle of 12 mm diameter of steel bar after 28 days respectively. Similarly, the highest bond strength pattern of ECC inclusion with 1.5% and 2% was found by 31.12 MPa and 28.54 MPa at 0.05% of GO while the minimum bond strength pattern of ECC inclusion with 1.5% and 2% was noted by 19.98 MPa and 18.30 MPa at 0.08% of GO particle of 12 mm diameter of reinforcement steel bar for 28 days respectively. Finding has been displayed that the bond strength of GO-ECC reinforced with 1% PVA fibre is providing maximum output as compared to the bond strength of GO-ECC blended with 1.5% and 2% of PVA fibre after 28 days consistently. In the same way, the optimum

Table 4 – Outcomes of pull-out test.

Mix ID	Steel reinforcement Bar 12 mm diameter				Steel reinforcement Bar 16 mm diameter			
	Optimum pull out load (KN)	Bond strength (MPa)	Bond energy (N-mm)	Bond slip (mm)	Optimum pull out load (KN)	Bond strength (MPa)	Bond energy (N-mm)	Bond slip (mm)
M1	126.66	31.12	495.767	2.35	161.8575	22.37	339.851	1.45
M2	94.84	23.30	290.697	2.75	137.1825	18.96	274.075	1.88
M3	97.43	23.94	345.929	2.58	149.34	20.64	334.191	1.70
M4	81.30	19.98	337.233	2.86	129.20	17.85	232.085	1.92
M5	97.43	23.94	345.929	2.58	149.34	20.64	334.191	1.70
M6	141.09	34.67	503.157	1.52	178.815	24.72	496.164	1.38
M7	116.14	28.54	324.402	2.48	159.09	21.99	309.582	1.65
M8	98	24.08	346.24	2.59	150	20.73	335.215	1.71
M9	157.50	38.70	722.631	1.22	183.30	25.34	544.258	1.15
M10	98.4	24.18	345.929	2.59	150.2	20.76	334.191	1.70
M11	126.76	31.15	460.47	2.02	177.28	24.50	367.848	1.75
M12	97.8	24.03	345.98	2.57	149.4	20.65	334.320	1.71
M13	74.505	18.30	207.081	2.95	116.675	16.12	174.305	2.05

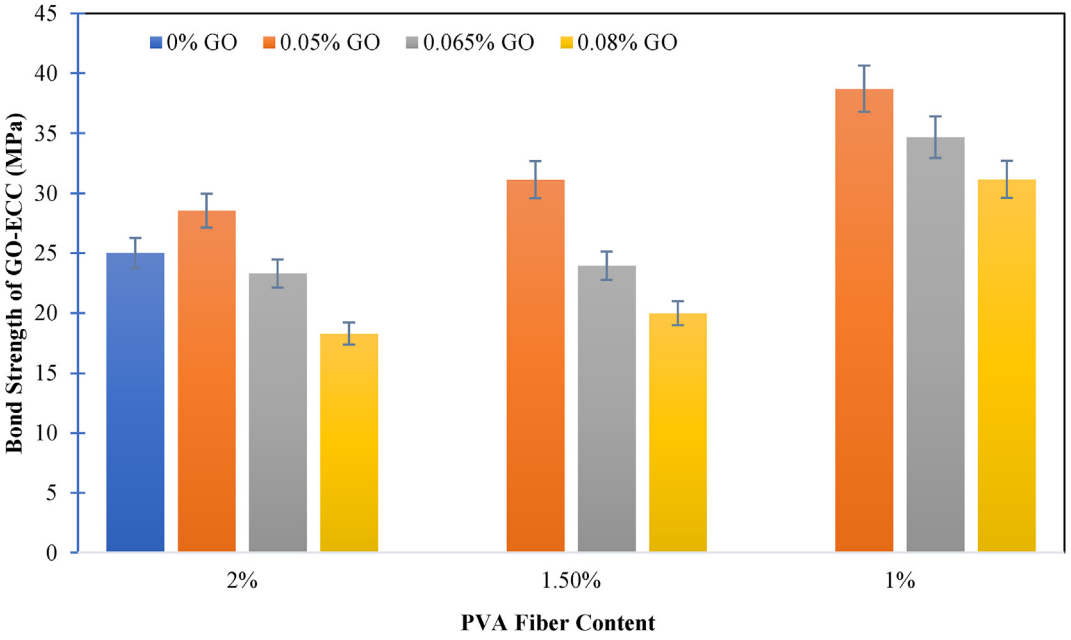

Fig. 6 – Bond Strength of GO-ECC mixture of 12 mm diameter steel bar.

pull-out strength of ECC reinforced with 1% PVA fibre was noted by 25.34 MPa at 0.05% of GO particle while the smallest pull out strength of ECC blended with 1% of PVA fibre was recorded by 24.50 MPa at 0.08% GO particle of 16 mm diameter of steel bar at 28 days respectively. Besides, the highest bond strength pattern of ECC inclusion with 1.5% and 2% was found by 22.37 MPa and 21.99 MPa at 0.05% of GO while the minimum bond strength pattern of ECC inclusion with 1.5% and 2% was noted by 17.86 MPa and 16.13 MPa at 0.08% of GO particle of 16 mm diameter of reinforcement steel bar for 28 days respectively. It was determined that the bond strength of GO-ECC blended with various content of PVA fibres is getting decreased with increased the diameter of steel reinforcement bar. Similar trend was observed in Ref. [65]. The outcome of bond strength of GO-ECC reinforced with several proportions of PVA fibre is dropped while increasing in the diameter of steel reinforcement bar. The bond strength of GO-ECC of 16 mm diameter of steel bar is recorded lower as compared to the bond strength of GO-ECC blended with several

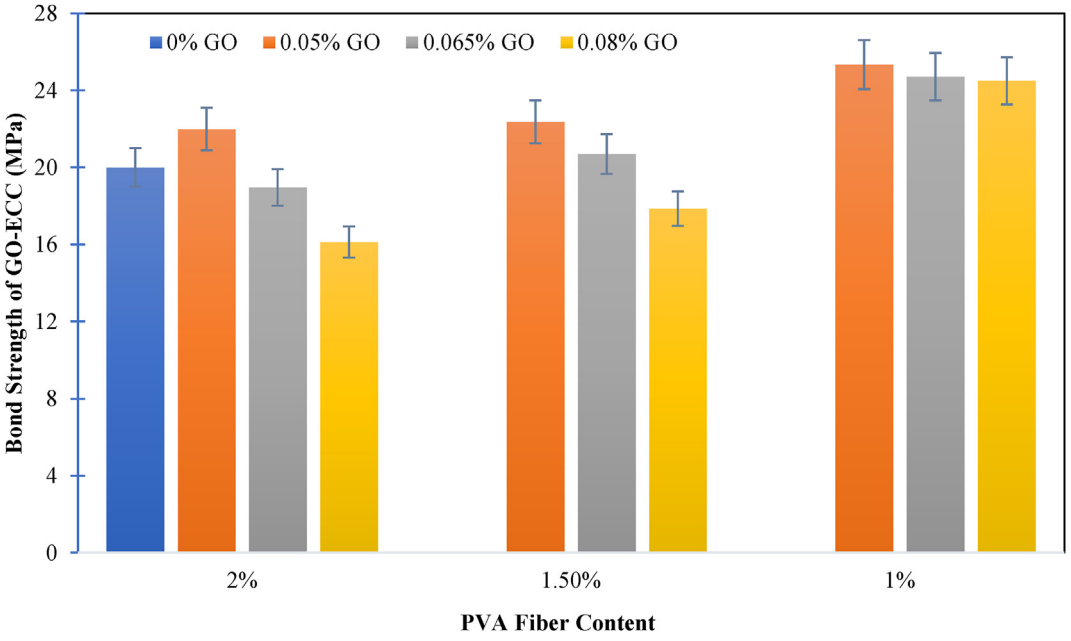

Fig. 7 – Bond Strength of GO-ECC mixture of 16 mm diameter steel bar.

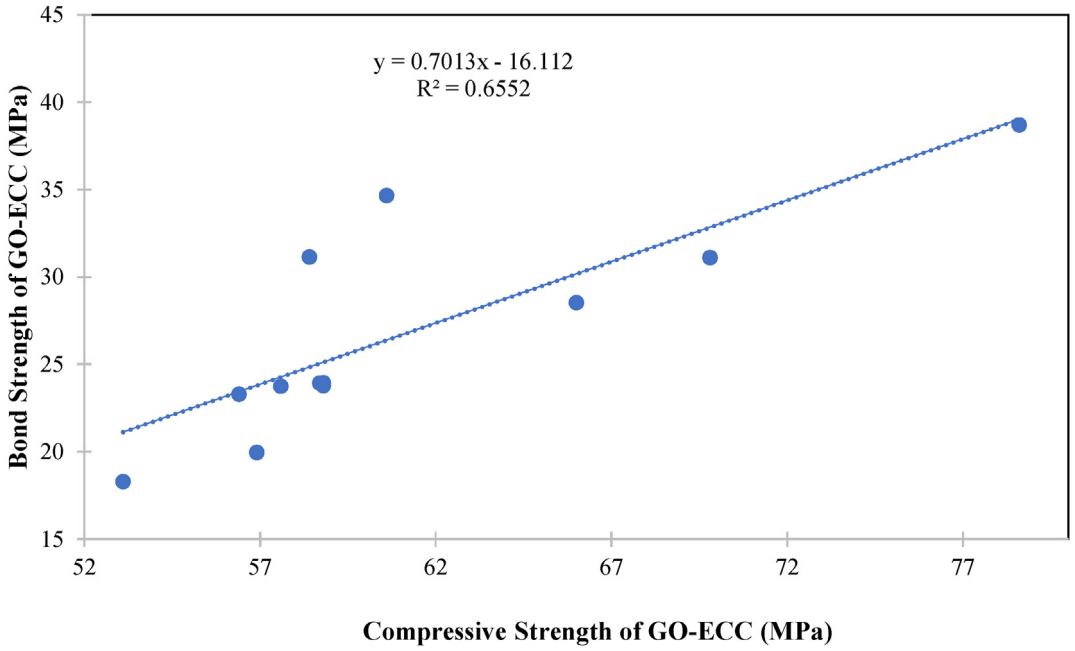

Fig. 8 – Correlation between bonding strength and compressive strength of GO-ECC of 12 mm diameter of steel bar.

content of PVA fibre of 12 mm diameter of steel reinforcement bar. The drop in bond strength caused by increasing reinforcement diameter of Steel bar is attributable to a decrease in limiting impact and concrete cover size [38]. The size of the concrete cover influences the confining mechanisms that govern bond tensions. The increased concrete cover in a lesser diameter bar adds to better confinement and, as a result, stronger bond strength [37,66]. A rise in the effect region related to an enhance in the diameter of steel rod without a corresponding rise in dimensions of the sample can contribute to the number of radial stresses surrounding the ribs, thereby changing the mechanism of failure to fracturing [65]. Figs. 8 and 9 display the strong correlation between the bond strength of GO-ECC blended with various proportions of PVA fibre of 12 and 16-mm diameter of steel bar and compressive strength of GO-ECC reinforced with several content of PVA fibre after 28 days respectively. The equation in Figs. 8 and 9 may be applied to calculate the bond strength of GO-ECC reinforced with 1%–2% of PVA fibre of 12 and 16-mm diameter of steel bar or compressive strength of GO-ECC blended with several content of PVA fibre while one characteristic strength of them is

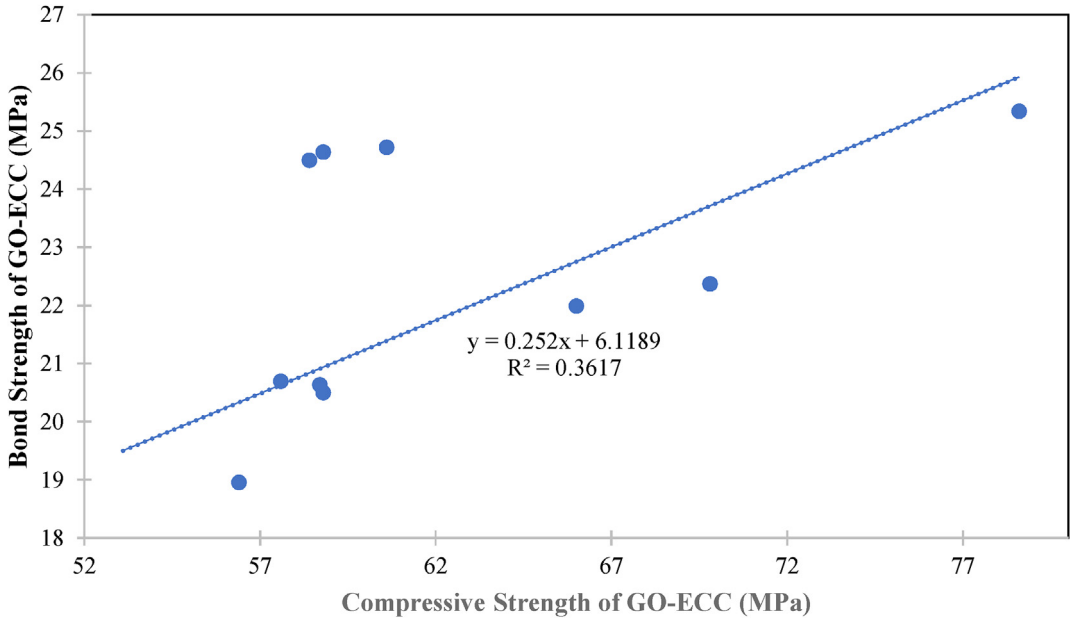

Fig. 9 – Correlation between bonding strength and compressive strength of GO-ECC of 16 mm diameter of steel bar.

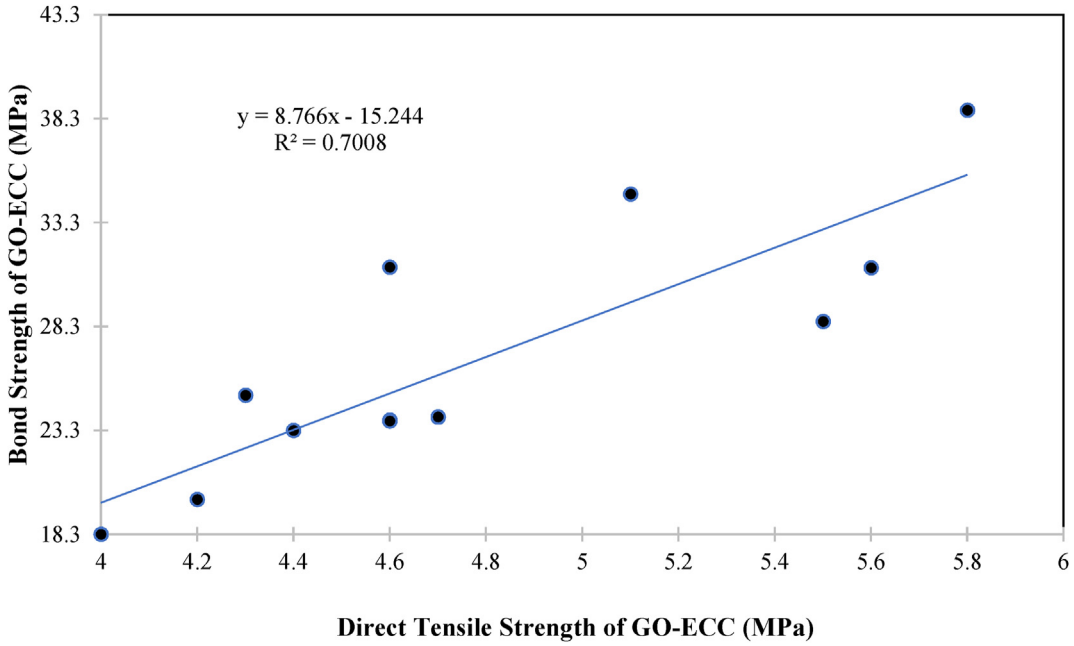

Fig. 10 – Correlation between bonding strength and direct tensile strength of GO-ECC of 12 mm diameter of steel bar.

known. In addition, Figs. 10 and 11 show the significant relationship between the bond strength of GO-ECC reinforced with different amounts of PVA fibre after 28 days and the tensile strength of GO-ECC reinforced with different amounts of PVA fibre after that time, respectively. The bond strength of GO-ECC reinforced with 1%–2% of PVA fibre of 12 and 16-mm diameter steel bars or the tensile strength of GO-ECC blended with various contents of PVA fibre may both be calculated using the equations in Figs. 10 and 11, provided that one of their characteristic strengths is known.

4.6. *Bond stress slip behaviour of GO-ECC*

Figs. 12–14 displayed the 12 mm diameter reinforcement steel rod implanted in GO-ECC mixes combined with varied quantities of PVA fibre show nominal stress against end slip displacement outcomes of pull-out samples. Table 4 summarises nominal stress vs. end slip for reinforcement steel rod with diameters of 16 mm. The bond stress was calculated as the area that lies below the bond stress-slip curve, and the mean pull-out forces of three samples for every diameter size

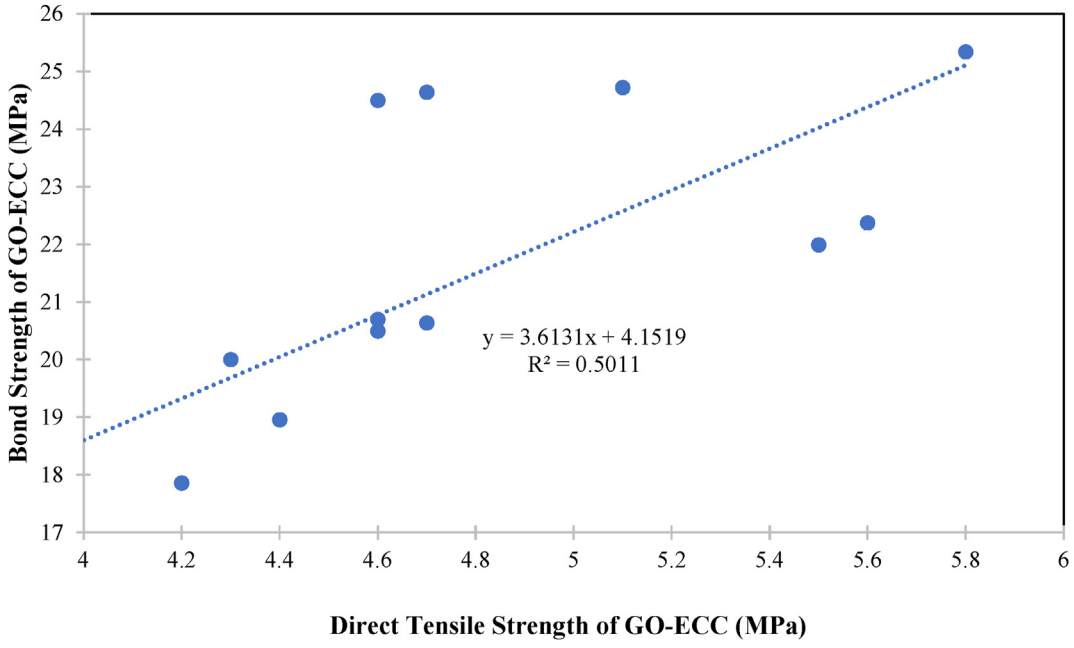

Fig. 11 – Correlation between bonding strength and direct tensile strength of GO-ECC of 16 mm diameter of steel bar.

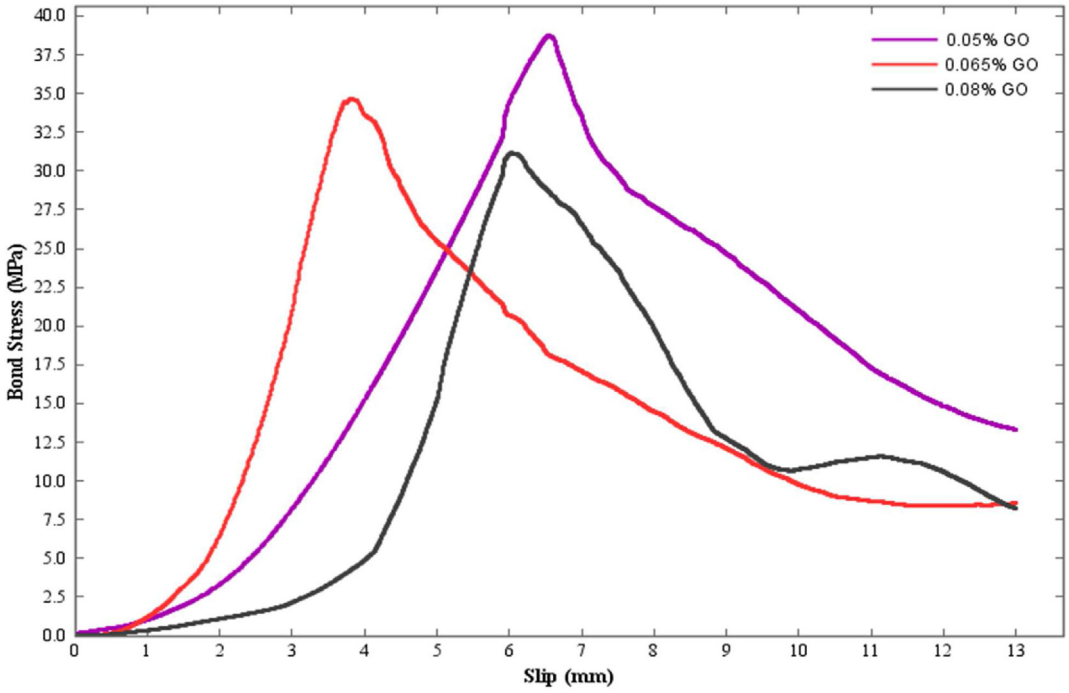

Fig. 12 – Bond Stress of GO-ECC blended with 1% of PVA fibre of 12 mm diameter of Steel bar.

were used to calculate the bond's energy. The maximum bond stress in a bond stress-slip curve was also employed to calculate the bond strength. Similarly, the end slip was calculated by averaging the LVDT and LPVT values obtained throughout the pull-out tests. Table 6 lists the bonding energy, optimum bonding strength, and bonding slip at the highest bonding strength of steel bars in two distinct diameters (12 mm and 16 mm), as calculated from the pull-out reactions of GO-ECC reinforced with various percentages of PVA fibre.

For each given percent of PVA fibre mixes, the effects of various GO nanoparticle concentrations are examined. Using 0.05% of GO nanoparticles for mixes of 1.0%, 1.5%, and 2% PVA fibres increases the final bond stress (bond strength), as seen in Figs. 12–14, but corresponding slips at the same stress level

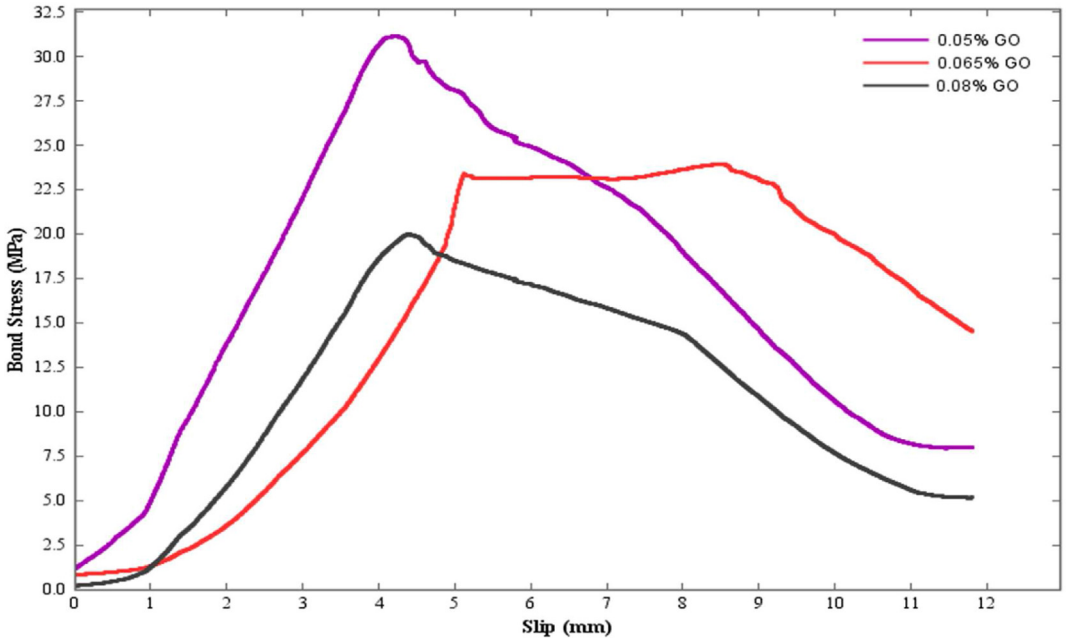

Fig. 13 – Bond Stress of GO-ECC blended with 1.5% of PVA fibre of 12 mm diameter of Steel bar.

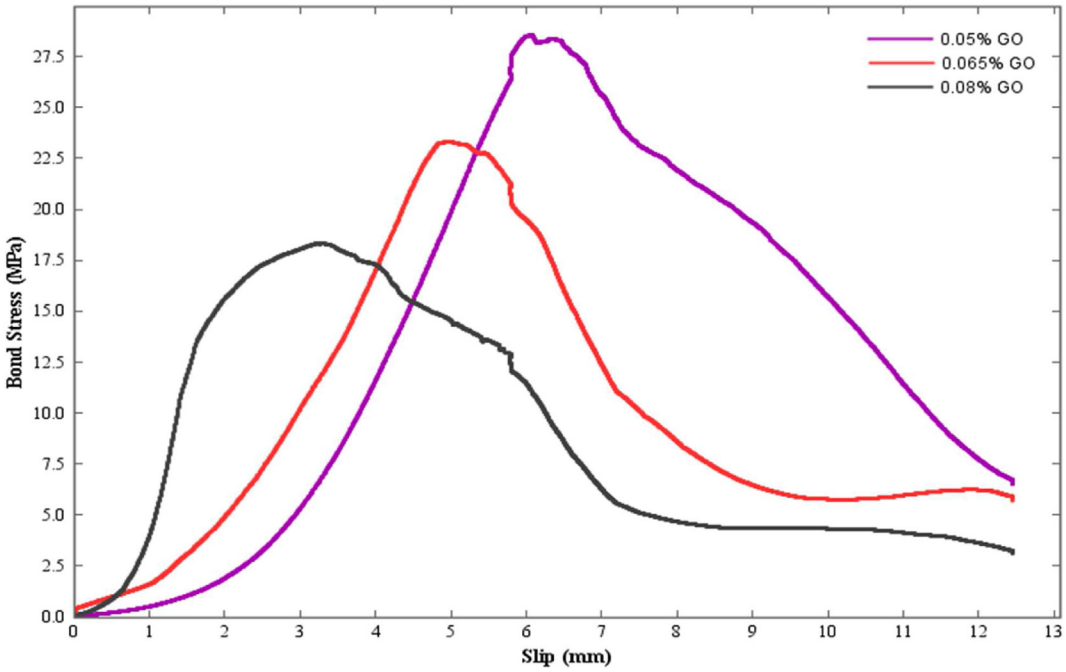

Fig. 14 – Bond Stress of GO-ECC blended with 2% PVA fibre of 12 mm diameter of Steel bar.

reduce. The binding energy improved for these mixes in a similar manner. For example, when up to 0.05% of GO particles were added to 1% PVA fibre, the bond energy improved. Moreover, GO nanoparticles and PVA fibres worked together to enhance the fibre-matrix interface, which encouraged GO-ECC to exhibit strain-hardening characteristics throughout the pull-out experiment. On the samples' surface, further microscopic cracks were seen. As a consequence, the energy released through the de-bonding of the fibres is enhanced. The area under the curve was enhanced by the many micro-cracks and the strain-hardening tendency [13]. The enhanced component hardness, which prevents splitting fractures by fibre bridging of cracks, is responsible for the higher bonding energy and bonding slip of the GO-ECCs [13]. The stability of a structure is enhanced by this tendency.

5. Response surface methodology and multivariate optimization

The non-linear response of ECC, concrete as well as cementitious ingredients as a result of a series of variations in their component ingredients and manufacturing techniques necessitates the resolution of non-linear optimization issues [67]. The RSM is diagrammatic description of responses acquired via the use of one or even more parameters in mathematical or statistical modelling techniques [68]. The response surface (RS) evaluates the impact and relevance of each parameter. Several cement and concrete qualities have been optimized using the RSM [69–71]. The mixture's constituents serve as independent variables in the concrete matrix, while the concrete's characteristics serve as dependent indicators. Building response surface of the investigational information and the matching model that most closely fits the information are required for the application, which is then followed by a determination of the model's accuracy [69,70]. A response surface may easily describe the whole system after defining the empirical relationship between at least two independent variables and one dependent variable (response) [67]. The graphical response allows you to clearly identify the independent factors that influence the overall system. After identifying the important independent variables, the approximate solution to the answer is achieved. A model must be created in order to optimize the experimental variables. The RS is optimized to provide the optimal answer for the response parameters. A generic, optimum solution to the problem must be produced using the model. Develop a model necessitates the collection of experimental evidence [69]. Multi-objective optimization issues exist in a variety of domains, including the aircraft industry, oil and gas sector, vehicle design, the financial sector, product and process design, or anywhere optimum choices must be made in the middle of competing goals, including trade-offs [72]. Examples of multiobjective optimization concerns are: maximizing benefits and minimizing the price of the product; a vehicle's fuel consumption is minimised by decreasing weight while improving a specific component's strength, increasing the ECC's Young's modulus, improving compressive strength, and maintaining the requirements of micromechanics [61,72].

5.1. *Experimental design in RSM*

Analysis of variance (ANOVA) was used to fit a quadratic model to the response surface technique. The responses that are analysed and considered include bond strength (ultimate bonding stress), bonding energy and bonding slip. A strategy

Table 5 – Experimental design of GO-ECC mixture by applying RSM.

Run	Factor 1 A: PVA (%)	Factor 2 B: GO (%)	Response 1 Bond strength (MPa)	Response 2 Bond slip (mm)	Response 3 Bond energy (N-mm)
1	1.5	0.065	23.9425	2.58	345.929
2	2	0.065	23.306	2.75	290.697
3	1.5	0.065	23.9425	2.58	345.929
4	1	0.08	31.1492	2.02	460.47
5	1.5	0.065	23.9425	2.58	345.929
6	1	0.065	34.6706	1.52	503.157
7	2	0.05	28.5389	2.48	324.402
8	1.5	0.05	31.1265	2.35	495.767
9	1	0.05	38.7031	1.22	722.631
10	1.5	0.065	23.9425	2.58	345.929
11	1.5	0.08	19.98	2.86	337.233
12	1.5	0.065	23.9425	2.58	345.929
13	2	0.08	18.3084	2.95	250

for multi-objective optimization based on response models from RSM is provided. The GO and PVA proportions were chosen as independent variables (factors) in this technique. According to available experimental information as well as trial combinations, the collection of independent variables is selected. Table 5 shows the several combinations of variables as well as the associated responses such as bond strength, bond energy and slip for GO-ECC mixes provided in RSM design. Samples were prepared and assessed for each response at the age of 28 days.

5.2. *Response predictive mathematical models*

The RSM was applied to generate the optimum predictor statistical approach shown in Equation (1) in order to establish the ideal situations for the different replies [73].

Table 6 – ANOVA outcomes.

Response	Source	Sum of Squares	Df	Mean Square	F-Value	p-value > F	Significance
Bond Strength	Model	412.20	5	82.44	186.21	<0.0001	**Yes**
	A-PVA	196.88	1	196.88	444.69	<0.0001	**Yes**
	B-GO	139.50	1	139.50	315.09	<0.0001	**Yes**
	AB	1.79	1	1.79	4.05	0.0842	**No**
	A^2	52.46	1	52.46	118.50	<0.0001	**Yes**
	B^2	2.35	1	2.35	5.32	0.0545	**No**
	Residual	3.10	7	0.44			
	Lack of Fit	3.10	3	1.03			
	Pure Error	0.000	4	0.000			
	Cor Total	415.29	12				
Bond Slip	Model	3.11	5	0.62	384.02	<0.0001	**Yes**
	A-PVA	1.95	1	1.95	1205.23	<0.0001	**Yes**
	B-GO	0.53	1	0.53	326.48	<0.0001	**Yes**
	AB	0.027	1	0.027	16.83	0.0046	**Yes**
	A^2	0.54	1	0.54	332.66	<0.0001	**Yes**
	B^2	2.262E-003	1	2.262E-003	1.40	0.2755	**No**
	Residual	0.011	7	1.617E-003			
	Lack of Fit	0.011	3	3.774E-003			
	Pure Error	0.000	4	0.000			
	Cor Total	3.12	12				
Bond Energy	Model	1.823E+005	5	36463.96	75.26	<0.0001	**Yes**
	A-PVA	1.124E+005	1	1.124E+005	231.95	<0.0001	**Yes**
	B-GO	40853.51	1	40853.51	84.32	<0.0001	**No**
	AB	8813.36	1	8813.36	18.19	0.0037	
	A^2	3867.73	1	3867.73	7.98	0.0256	**No**
	B^2	8971.77	1	8971.77	18.52	0.0036	
	Residual	3391.65	7	484.52			
	Lack of Fit	3391.65	3	1130.55			
	Pure Error	0.000	4	0.000			
	Cor Total	1.857E+005	12				

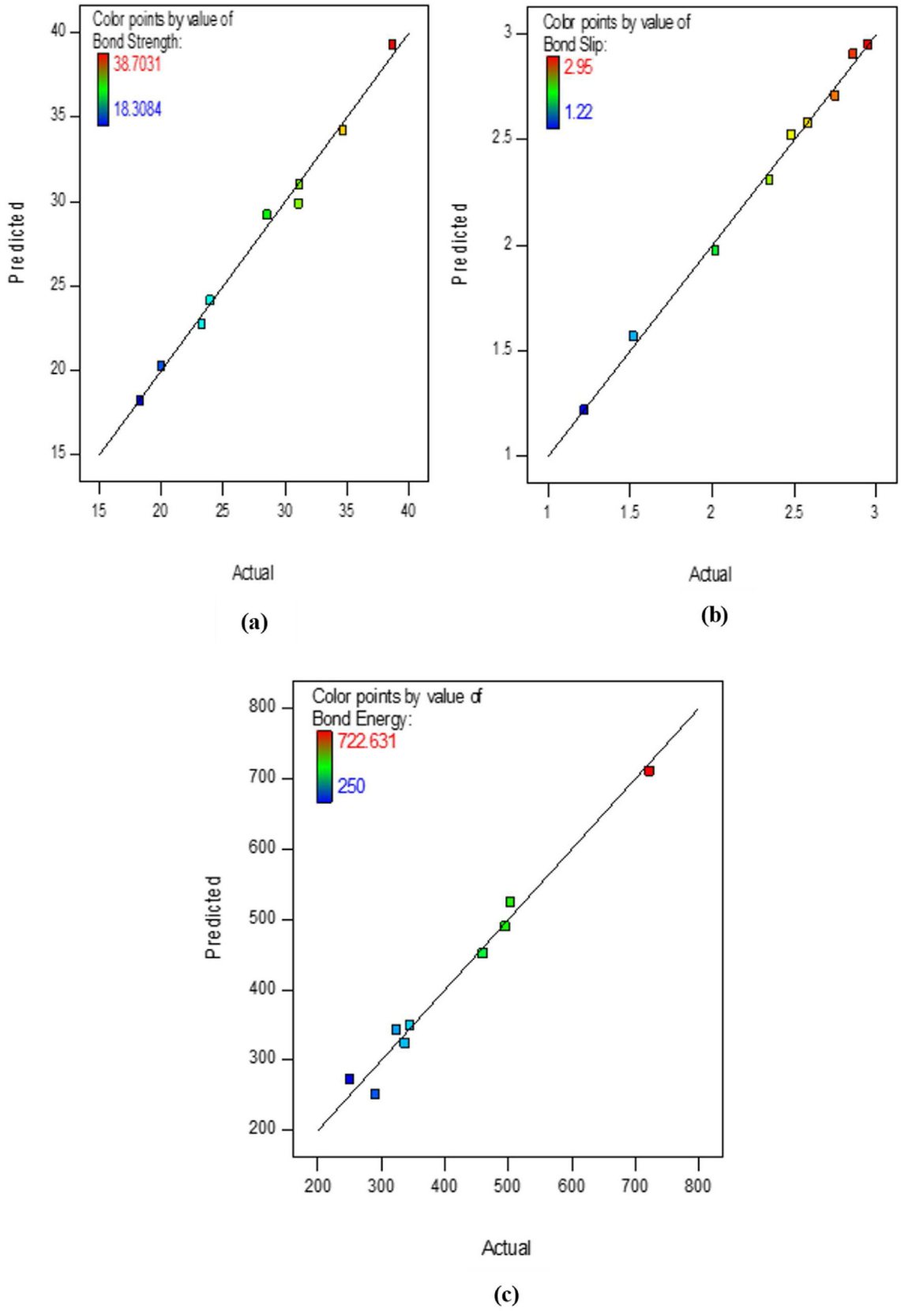

Fig. 15 – Predicted versus Actual Plots for (a) Bond Strength, (b) Bond Slip, (c) Bond Energy for 12 mm diameter of steel bar.

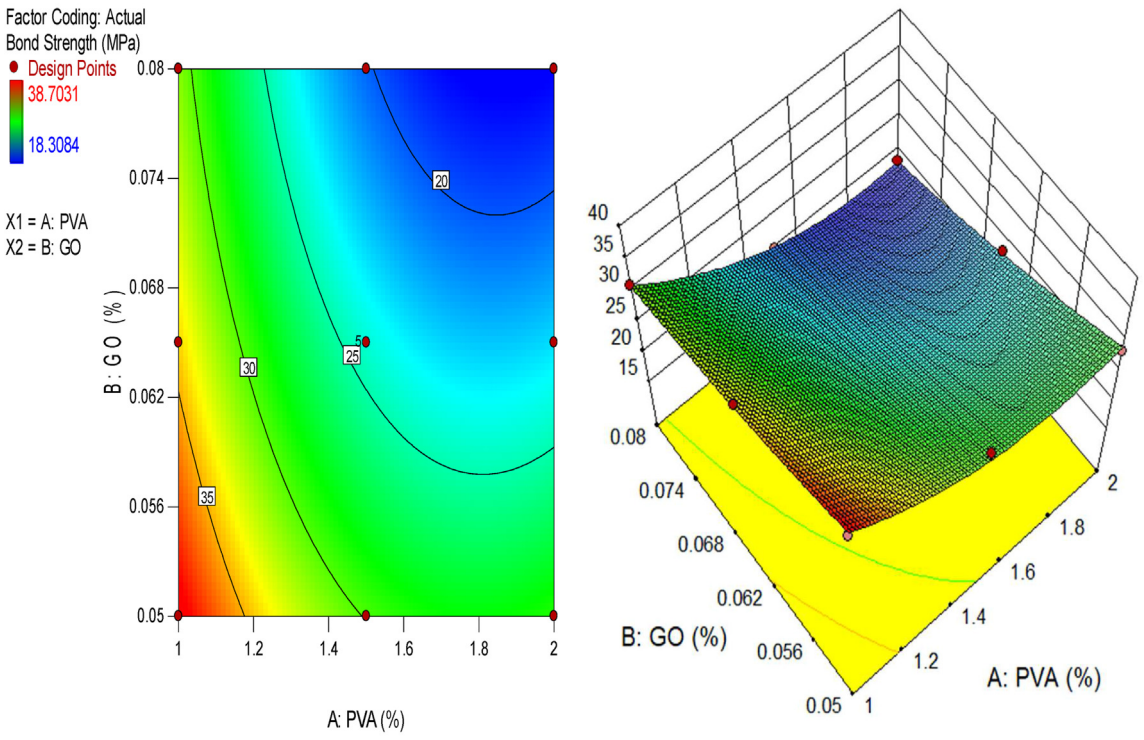

(a) (b)

Fig. 16 – (a) 2D contour plot and (b) 3D response surface diagram for Bond Strength.

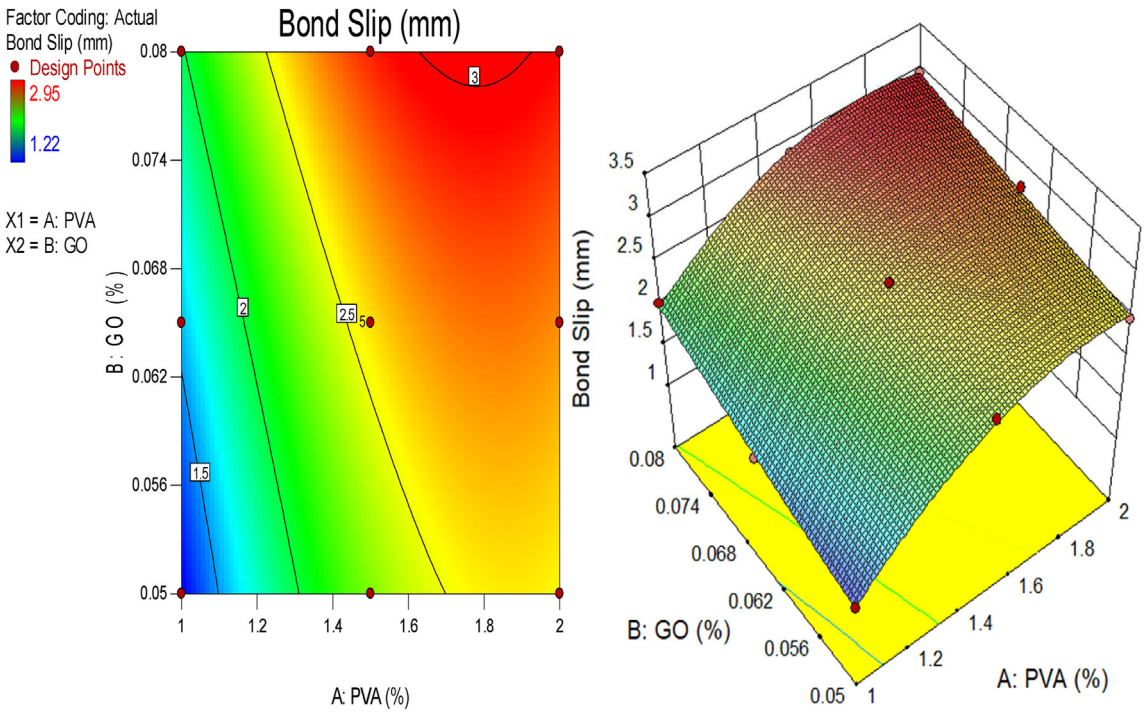

(a) (b)

Fig. 17 – (a) 2D contour plot and (b) 3D response surface diagram for Bond Slip.

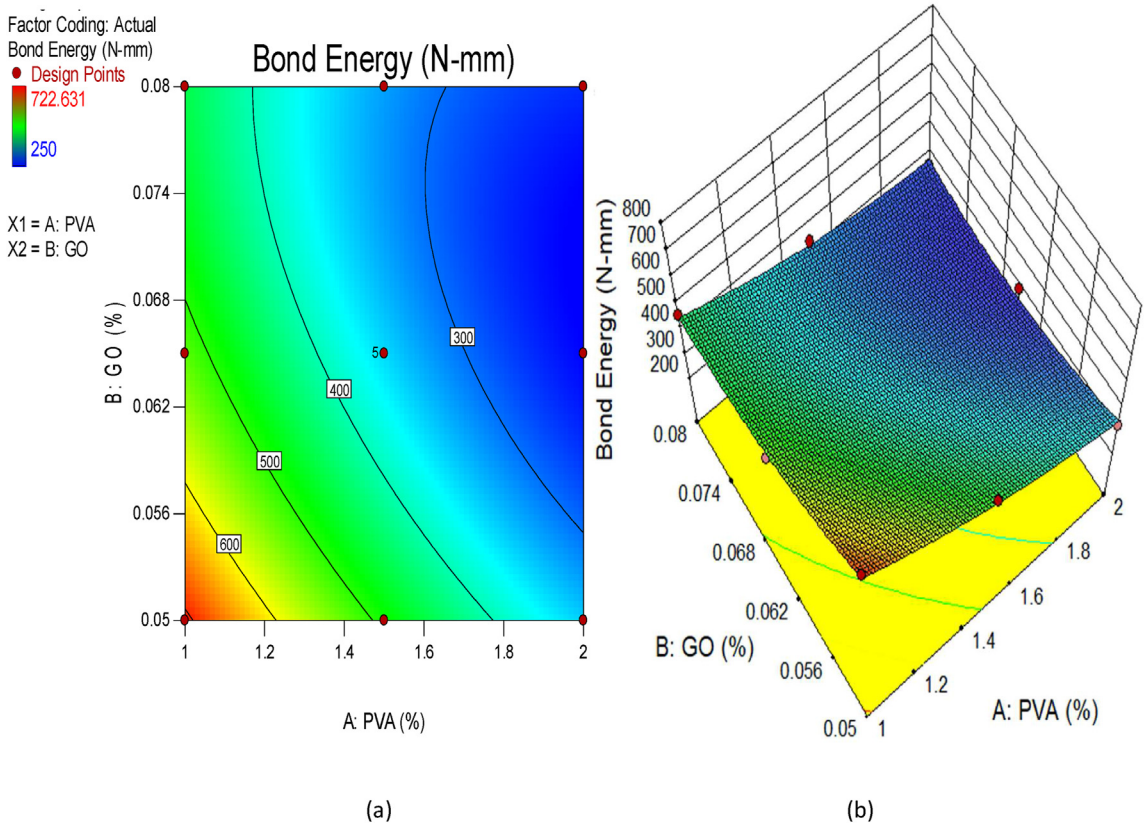

Fig. 18 – (a) 2D contour plot and (b) 3D response surface diagram for Bond Energy.

$$y = \beta_0 + \sum_{i=1}^{k} \beta_i x_i + \sum_{i=1}^{k} \beta_{ii} x_i^2 + \sum_{j=2}^{k} \sum_{i=1}^{j=1} \beta_{ij} x_i x_j + \varepsilon \quad (1)$$

The responses were independently analysed, and a model (quadratic) was chosen based on an examination of summary graphs information for the important factors. The 2D and 3D plots were used to determine the appropriateness of the proposed models. In order to determine the accuracy of the models' predictions, their R^2 coefficients are evaluated. The probability was used to validate the model parameters with a 95% degree of assurance and a 5% level of significance. The parameter with a probability value that was not statistically significant were deleted, with the exception of those necessary to preserve the model's term hierarchy. Furthermore, the investigational information was fitted to quadratic types of statistical models, guaranteeing a representation of the relationship between the predicted and the investigational results by adjusting the model's parameters.

5.3. *Analysis of variance (ANOVA)*

The ANOVA in Table 6 demonstrates that the bonding slip, bonding strength, and bonding energy are correlated. For each outcome, the difference between the adjusted R^2 and the expected R^2 is significantly less than 0.2. This suggests there is a

Table 7 – Specifications for model validation.

Model Validation Constraints	Bond Strength	Bond Slip	Bond Energy
Standard Deviation	0.67	0.040	22.01
Mean	26.58	2.39	393.38
Coefficient of Variance (%)	2.50	1.68	5.60
PRESS	26.85	0.12	32696.59
−2 Log Likelihood	18.25	−54.70	109.23
R^2	0.9925	0.9964	0.9817
Adj R^2	0.9872	0.9938	0.9687
Pred R^2	0.9354	0.9631	0.8239
Adeq Precision	46.678	63.440	30.772
BIC	33.64	−39.32	124.62
AICc	44.25	−28.70	135.23

Table 8 – Optimization goals and results.

Factors		Input Factors		Responses (Output Factors)		
		GO (%)	PVA (%)	Bond Strength (MPa)	Bond Slip (mm)	Bond Energy (N-mm)
Value	Minimum	0.05	1	18.30	1.22	722.63
	Maximum	0.08	2	38.70	2.95	250
Goal		Range	Range	Maximize	Minimize	Minimize
Optimization Results		0.05	1.00	39.30	1.21	710.54
Desirability				0.991 (99.10%)		

strong correlation between the investigational and predicted information. In addition, the desired limit is shown by the ratio of signal to noise of suitable accuracy being well above 4, which also approves that models may be utilised to travel within the user-defined design space of the RSM. ANOVA in Table 6 is also used, with a significance level of $p < 0.05$, to evaluate the significance value of the approaches and model variables (PVA fibre and GO) for different responses like bonding strength, bonding energy and bonding slip. In these instances, A, B, AB, A^2 and B^2 are key parameters for models of bonding strength, bonding slip, and bonding energy response. This suggests that the major model terms are enhancing the design approach. The model factors with a probability value greater than 0.05 were deemed statistically insignificant and were consequently eliminated, with the exception of those necessary to preserve the model's hierarchical structure. The PVA fibres were responsible for the majority of the decrease in bond energy as well as bond strength, while decreasing in bond slip, whereas GO particles were responsible for the quadratic impact. Fig. 15 depicts the comparison between the predicted and actual values of the responses in order to further validate the appropriateness of the models. All of the points on the actual vs. predicted plots for the responses fell along the straight line, indicating high agreement. This verifies that the models may be utilised to get about the area of design effectively. Bonding strength, bonding slip, and bonding energy were calculated using the quadratic model as specified in the software depend on input factors. The models were chosen depending on the non-aliased sum of squares of a polynomial of greater order, and the variables in the mathematical framework were statistical significance.

5.4. *Finding the research parameters through RSM modelling*

The RSM may be visually represented by plotting the output as a purpose of two factors (GO nanoparticles and PVA fibre). Figs. 13–15 depict the 2D and 3D response surface analyses of the determined GO-ECC parameters for bonding strength, bonding slip, and bonding energy of an ECC mixture blended with various contents of PVA fibre in a pull-out steel reinforcement bar having a 12 mm diameter. The 2D and 3D response surface plots highlight the effects of the independent variables (GO nanoparticles and PVA fibre) proportions on the bonding energy, bonding slip and bonding strength responses. These graphs show the influence of GO nanoparticles and PVA fibres on the investigational circumstances of the outcomes. It is clear that the impact of PVA fibres on the

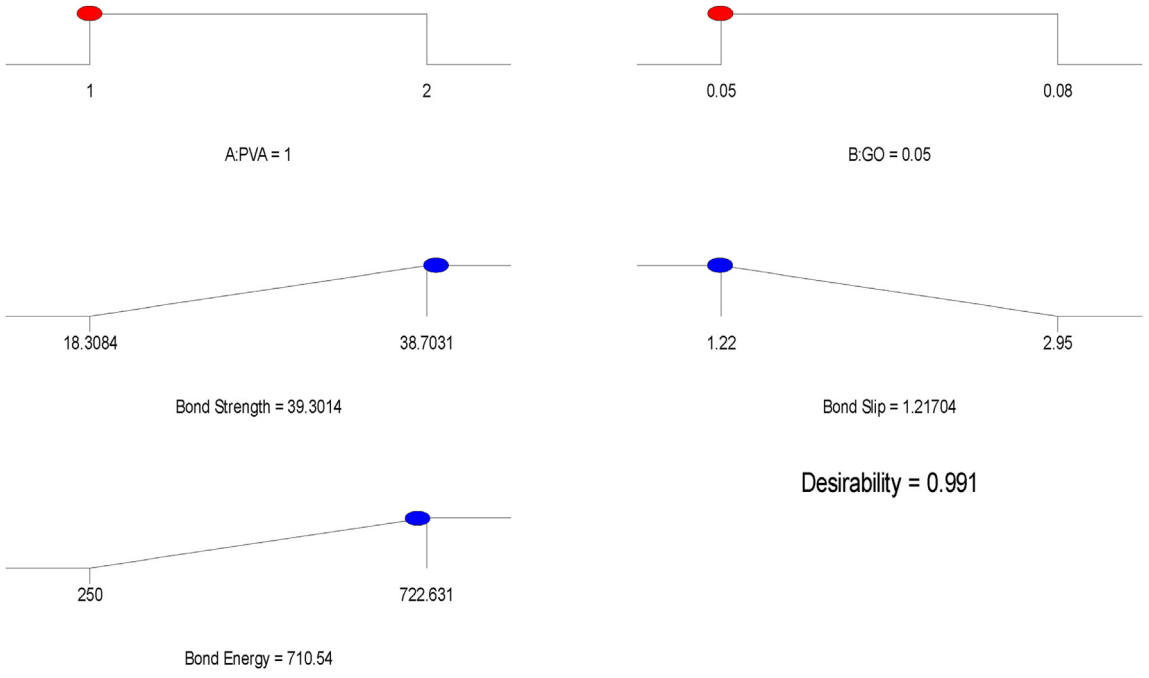

Fig. 19 – Optimization solution ramp.

responses is greater than that of GO nanoparticles. The contours and sloped lines depict the relationship between the independent factors. Nevertheless, the functional relationships among the factors had a bigger impact on the outcomes owing to their synergistic significance.

Figs. 16–18 depict three-dimensional response diagrams of bonding slip, bonding strength, and bonding energy were assessed from pull-out measurements of steel reinforcement rod having 12 mm diameter implanted in GO-ECC samples as a consequence of PVA fibres and GO nanoparticles. According to the ANOVA results, a nonlinear relationship was formed among the bonding slip, bonding energy, and bonding strength, as well as the PVA fibre content and GO proportions. The 3D RSM graphs in Fig. 16 (b) and 18 (b) reveal that as the proportions of PVA fibres rise in the ECC mixture, that results in reducing the bonding energy and bonding strength, but increases the bonding slip, while the 0.05% of GO used as a nanoparticle in ECC increases the bonding strength and bonding energy. With more accumulation of GO particles to ECC, the bonding strength and bonding energy start reducing. The cumulative impact of PVA fibres and GO nanoparticles resulted in increased bonding energy and strength after 28 days correspondingly. Moreover, the bonding strength and bonding energy of ECC combination comprising 1% PVA fibres and 0.05% GO nanoparticles was obtained optimum as compared to the other mixtures. Besides, the bond slip is noted reduced at 0.05% of GO along with 1% of PVA as compared to the other mixture. As a result, the maximum improvements in bond strength and bond energy that can be produced with PVA fibres and GO nanoparticles are 39.30 MPa and 750 N-mm, correspondingly, while the lowest reduction in bonding slip was 1.96 mm, achieved from a combination containing 1% PVA fibres and 0.05% GO nanoparticles. Though the amount of 1% PVA fibres along with 0.05% GO nanoparticles boosts bond strength, it would also influence the ductile characteristics, strain-hardening, and various fracture behaviours of GO-ECC, potentially resulting in a material loss of resilience.

The above-mentioned impact may be seen in the 2D plots (Figs. 16–18), which are used to assess the impact on outcomes of GO-ECC characteristics. A variables curve, beginning from the reference value, demonstrates that the model anticipates the response is going to change when the parameter is increased or decreased in the mixture. In the instance of bonding strength and bonding energy, the steady rise in the proportions of PVA fibre and GO nanoparticles from a minimal concentration (information encoded - 1) to a higher one (information encoded + 1) resulted in an enhance and consequent drop in bonding strength and bonding energy. Moreover, the bonding slip is going to increase when the ratios of PVA fibre and GO nanoparticles are raised. According to the 2D plots in Figs. 16–18, the usage of 2% PVA fibres and 0.08% GO nanoparticles caused the greatest increase. Nevertheless, a significant loss in bond strength and bond energy was seen in excess of this percentage, even though a rise in bond slip was reported. The impact of the PVA fibre and the GO nanoparticles may be connected to the change in bonding slip, bonding strength, and bonding energy of mixes with varying PVA fibre and GO particle proportions. After 2%, the fraction of GO nanoparticles may surpass the threshold of accessible

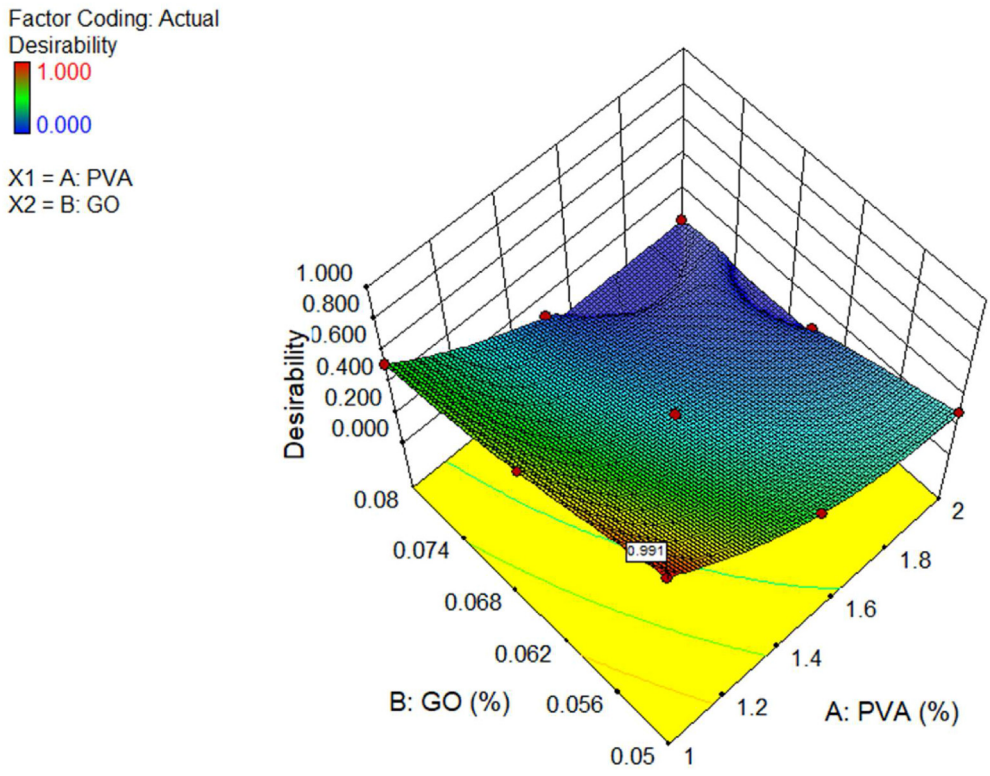

Fig. 20 – 3D diagram for the desirability of the optimization.

Table 9 – Experimental validation.

Responses	Experimental Outcomes	Predicted Outcomes	Percentage Error (%)
Bond Strength (MPa)	38.703	39.301	1.545
Bond Energy (N-mm)	722.631	710.54	1.673
Bond Slip (mm)	1.22	1.217	0.246

calcium hydroxide response in the ECC mixture. This may also have an impact on the homogeneous distribution of PVA fibre in the mixture, the subsequent efficient development of numerous fractures, and the strain-hardening activity of the GO-ECC. In accordance with Table 7, the variance between the adjusted and predicted R^2 readings is lower than 0.20, and suggesting the model is quite accurate. The standard deviation (SD) is below 5.0%.

5.5. *Optimization for multiple responses using RSM*

The technique of multi-objective optimization involves the continuous evaluation of multiple linear regressions for outputs [74]. Table 8 describes the goals and requirements for the optimization of this incident. According to Table 8, the objective of optimization is to maximize two answers and minimize one output. Equations (2)–(4) show and describe the correlation between the independent factors (GO nanoparticles and PVA fibre) of the ECC mixes and their observed predictor variables. Using multi-objective optimization, the optimal situations for the independent factors that may create the response situation were determined. After building the regression model between the parameters of the design mix and the outputs, all parameters were concurrently and individually modified to optimize the performance parameters. These optimum approach parameters attempt to fulfil the needs of each response without sacrificing any of the needs unduly [75]. The independent variables of the GO-ECC mixes are concurrently adjusted to optimize the objective functions separately and continuously. The goal of optimization is to find the optimal settings for the independent factors so that the response (multi-objective) parameter may be optimized. Table 8 shows the criterion parameters for the GO-ECC mixes employed. For continuous optimization of the replies, an optimization strategy applying the mathematical approach and utilizing the desirability feature established for every response may be applied [2,76]. The limit of variance of the desirability functions is ranging from 0 to 1. However, individual desirability functions range from 0 to 1, with 0 being utterly undesirable and 1 being completely desired. Desirability values close to one reflect the worldwide best mixture of several criteria, implying that the responses are the objective values. The objective of a mathematical optimization strategy might be to apply mixed parameters or outputs. Depending on the provided criteria, there are different approaches to calculating the desirability function. The intended set of objectives for answers might be in the context of a lowest, optimum, target, or range. The multivariate optimization of the responses to build general solution parameters is conducted in the Design-Expert program using the criteria established in Table 5. To obtain an optimal GO-ECC solution that maximizes the potentials of structural resilience, greater attention should be placed on simultaneously maximizing bonding energy and bonding strength. While minimizing bonding slip. Figs. 19 and 20 illustrate the ramps of the optimum model parameters and the 3D desirability (D) generated from multi-objective optimization. The optimal solution is found from the ramps exhibited at PVA = 1% and GO = 0.05%, with the expected outcomes of bonding strength = 39.30 MPa, bonding energy = 710.54 N-mm, and bonding slip = 1.217 mm, assessed at a desirability rate of 0.991. Though, a durable GO-ECC may be realized with great values of bonding slip, bonding strength, and bonding energy at defined parameters of multivariate outcome optimization. However, the multi-variate optimization approach may be utilised to build a robust GO-ECC with the desired set of parameters and outputs required for the stated objectives.

$$Bond\ Strength = +24.14 - 5.73 \times A - 4.82 \times B - 0.67 \times AB + 4.36 \times A^2 + 0.92 \times B^2 \quad (2)$$

$$Bond\ Slip = +2.58 + 0.57 \times A + 0.30 \times B - 0.082 \times AB - 0.44 \times A^2 + 0.029 \times B^2 \quad (3)$$

$$Bond\ Energy = +349.81 - 136.86 \times A - 82.52 \times B + 46.94 \times AB + 37.42 \times A^2 + 56.99 \times B^2 \quad (4)$$

5.6. *Validation of the prediction model*

After using multivariate optimization to find the best projected solution for the parameters (A: PVA and B: GO), at least three samples of the GO-ECC combination shown in Fig. 5 were made and tested for pull-out. The GO-ECC combination was generated using the fixed mixture components listed in Table 3. Following the mixing process, at least 03 specimens were made for individually testing characteristic, and their averages were noted. Table 9 provides the average method used to investigate each testing factor and its related absolute relative deviation (ARD) from the predicted outcomes. The observed ARD were estimated using Equation (5), and the predicted model's precision was determined by evaluating each parameter [77]. The determined experimental and predicted findings in Table 9 are in excellent agreement due to the nominal variance. This verifies the predictability of the model.

$$ADR = \frac{Experimental\ Data - Predicted\ Data}{Experimental\ Data} \times 100 \quad (5)$$

6. Conclusions

This research studied the pull-out loads and related slips of two different diameters of steel reinforcing bars implanted in GO-ECC mixes. The bonding strength, bonding energy, and

bonding slip were calculated and analysed as performance measures. On the basis of the test findings and analyses conducted, the following inferences may be made.

- By integrating GO, an FA-to-cement ratio of roughly 1.2 might be used. This helps with cost savings because of the decreased cement consumption.
- The usage of GO nanoparticles in combination with PVA fibre in ECCs has an effect on the material's ductility and strain hardening properties. Pull-out versus slide charts demonstrate it. In the majority of graphs with PVA concentrations between 1% and 2%, the introduction of GO nanoparticles at 0.05% enhanced the area under the strain hardening curve.
- The proposed RSM regression model makes it easier to figure out the parameters of the bond-slip curve for GO-ECC samples with steel rebar of different diameters. Based on the p-value, the results of the ANOVA analysis also showed that all statistically important design variables were used. The best answers are found using 1% PVA fibres and 0.05% GO particles as design factors.
- The statistical models built via multivariate optimization make an excellent mix-design tool for calculating the quantities of GO-ECC required to acquire a set of desired characteristics.

Declaration of competing interest

The authors declare that they have no known competing financial interests or personal relationships that could have appeared to influence the work reported in this paper.

Acknowledgement

The Authors wish to acknowledge the support of Universiti Teknologi PETRONAS (UTP) Malaysia for funding the work under the grant with number: YUTP-FRG 1/2022 (015LC0-391).

REFERENCES

[1] Naaman AE, Reinhardt HW. Proposed classification of HPFRC composites based on their tensile response. Mater Struct Constr 2006;39:547–55. https://doi.org/10.1617/s11527-006-9103-2.

[2] Achara BE, Mohammed BS, Liew MS. Bond behaviour of nano-silica-modified self-compacting engineered cementitious composite using response surface methodology. Constr Build Mater 2019;224:796–814. https://doi.org/10.1016/j.conbuildmat.2019.07.115.

[3] Yang EH, Li VC. Tailoring engineered cementitious composites for impact resistance. Cement Concr Res 2012;42:1066–71. https://doi.org/10.1016/j.cemconres.2012.04.006.

[4] Yu K, Wang Y, Yu J, Xu S. A strain-hardening cementitious composites with the tensile capacity up to 8. Constr Build Mater 2017;137:410–9. https://doi.org/10.1016/j.conbuildmat.2017.01.060.

[5] Mohammed BS, Aswin M, Beatty WH, Hafiz M. Longitudinal shear resistance of PVA-ECC composite slabs. Structures 2016;5:247–57. https://doi.org/10.1016/j.istruc.2015.12.003.

[6] Lepech MD, Li VC. Application of ECC for bridge deck link slabs. Mater Struct Constr 2009;42:1185–95. https://doi.org/10.1617/s11527-009-9544-5.

[7] Caner A, Dogan E, Zia P. Seismic performance of multisimple-span bridges retrofitted with link slabs. J Bridge Eng 2002;7:85–93. https://doi.org/10.1061/(asce)1084-0702(2002)7:2(85).

[8] Qudah S, Maalej M. Application of Engineered Cementitious Composites (ECC) in interior beam-column connections for enhanced seismic resistance. Eng Struct 2014;69:235–45. https://doi.org/10.1016/j.engstruct.2014.03.026.

[9] Said SH, Abdul Razak H. Structural behavior of RC engineered cementitious composite (ECC) exterior beam-column joints under reversed cyclic loading. Constr Build Mater 2016;107:226–34. https://doi.org/10.1016/j.conbuildmat.2016.01.001.

[10] Said SH, Razak HA, Othman I. Flexural behavior of engineered cementitious composite (ECC) slabs with polyvinyl alcohol fibers. Constr Build Mater 2015;75:176–88. https://doi.org/10.1016/j.conbuildmat.2014.10.036.

[11] Khed VC, Mohammed BS, Liew MS, Alaloul WS, Adamu M, Al-Fakih A, Karthikeyan J. Experimental investigation on pullout strength of hybrid reinforcement of fibre in rubberized cementitious composites. Int J Civ Eng Technol 2018;9:1612–22.

[12] Li VC. On engineered cementitious composites (ECC). J Adv Concr Technol 2003;1:215–30. https://doi.org/10.3151/jact.1.215.

[13] Bandelt MJ, Billington SL. Bond behavior of steel reinforcement in high-performance fiber-reinforced cementitious composite flexural members. Mater Struct Constr 2016;49:71–86. https://doi.org/10.1617/s11527-014-0475-4.

[14] Beglarigale A, Yazici H. Pull-out behavior of steel fiber embedded in flowable RPC and ordinary mortar. Constr Build Mater 2015;75:255–65. https://doi.org/10.1016/j.conbuildmat.2014.11.037.

[15] Han B, Zhang L, Zeng S, Dong S, Yu X, Yang R, Ou J. Nano-core effect in nano-engineered cementitious composites. Compos Part A Appl Sci Manuf 2017;95:100–9. https://doi.org/10.1016/j.compositesa.2017.01.008.

[16] Zhang J, Wang Q, Zhang J. Shrinkage of internal cured high strength engineered cementitious composite with pre-wetted sand-like zeolite. Constr Build Mater 2017;134:664–72. https://doi.org/10.1016/j.conbuildmat.2016.12.182.

[17] Dreyer DR, Park S, Bielawski CW, Ruoff RS. The chemistry of graphene oxide. Chem Soc Rev 2010;39:228–40. https://doi.org/10.1039/b917103g.

[18] Zheng Q, Han B, Cui X, Yu X, Ou J. Graphene-engineered cementitious composites: small makes a big impact. Nanomater Nanotechnol 2017;7. https://doi.org/10.1177/1847980417742304.

[19] Yang H, Cui H, Tang W, Li Z, Han N, Xing F. A critical review on research progress of graphene/cement based composites. Compos Part A Appl Sci Manuf 2017;102:273–96. https://doi.org/10.1016/j.compositesa.2017.07.019.

[20] Sharma S, Kothiyal NC. Influence of graphene oxide as dispersed phase in cement mortar matrix in defining the crystal patterns of cement hydrates and its effect on mechanical, microstructural and crystallization properties. RSC Adv 2015;5:52642–57. https://doi.org/10.1039/c5ra08078a.

[21] Tong T, Fan Z, Liu Q, Wang S, Tan S, Yu Q. Investigation of the effects of graphene and graphene oxide nanoplatelets on the micro- and macro-properties of cementitious materials.

Constr Build Mater 2016;106:102–14. https://doi.org/10.1016/j.conbuildmat.2015.12.092.
[22] Al-Dahawi A, Yıldırım G, Öztürk O, Şahmaran M. Assessment of self-sensing capability of Engineered Cementitious Composites within the elastic and plastic ranges of cyclic flexural loading. Constr Build Mater 2017;145:1–10. https://doi.org/10.1016/j.conbuildmat.2017.03.236.
[23] Lin C, Wei W, Hu YH. Catalytic behavior of graphene oxide for cement hydration process. J Phys Chem Solid 2016;89:128–33. https://doi.org/10.1016/j.jpcs.2015.11.002.
[24] Chiranjiakumari Devi S, Ahmad Khan R. Influence of graphene oxide on sulfate attack and carbonation of concrete containing recycled concrete aggregate. Constr Build Mater 2020;250. https://doi.org/10.1016/j.conbuildmat.2020.118883.
[25] Zhu Y, Murali S, Cai W, Li X, Suk JW, Potts JR, Ruoff RS. Graphene and graphene oxide: synthesis, properties, and applications. Adv Mater 2010;22:3906–24. https://doi.org/10.1002/adma.201001068.
[26] Wang Q, Wang J, Lu C, Liu B, Zhang K, Li C. Influence of graphene oxide additions on the microstructure and mechanical strength of cement. Carbon N Y 2015;95:1083–4. https://doi.org/10.1016/j.carbon.2015.08.089.
[27] Sarabia LA, Ortiz MC. Response surface methodology. Compr Chemom 2009;1:345–90. https://doi.org/10.1016/B978-044452701-1.00083-1.
[28] Aydar AY. Utilization of response surface methodology in optimization of extraction of plant materials. Stat Approaches With Emphas Des Exp Appl Chem Process 2018. https://doi.org/10.5772/intechopen.73690.
[29] Bezerra MA, Santelli RE, Oliveira EP, Villar LS, Escaleira LA. Response surface methodology (RSM) as a tool for optimization in analytical chemistry. Talanta 2008;76:965–77. https://doi.org/10.1016/j.talanta.2008.05.019.
[30] Ferreira SLC, Dos Santos WNL, Quintella CM, Neto BB, Bosque-Sendra JM. Doehlert matrix: a chemometric tool for analytical chemistry-review. Talanta 2004;63:1061–7. https://doi.org/10.1016/j.talanta.2004.01.015.
[31] ASTM C150. In: Standard specification for Portland cement. West Conshohocken, PA, USA: ASTM International; 2015.
[32] ASTM C618-15. Standard specification for coal fly ash and raw or calcined natural pozzolan for use in concrete. West Conshohocken, PA, USA: ASTM International; 2015.
[33] Zhang Z, Yuvaraj A, Di J, Qian S. Matrix design of light weight, high strength, high ductility ECC. Constr Build Mater 2019;210:188–97. https://doi.org/10.1016/j.conbuildmat.2019.03.159.
[34] Mohammed BS, Achara BE, Liew MS, Alaloul WS, Khed VC. Effects of elevated temperature on the tensile properties of NS-modified self-consolidating engineered cementitious composites and property optimization using response surface methodology (RSM). Constr Build Mater 2019;206:449–69. https://doi.org/10.1016/j.conbuildmat.2019.02.033.
[35] BS EN 12390-3, Testing Harden Concrete. Compressive strength of test specimens. London, UK: BSI; 2009.
[36] Japan Society of Civil Engineers. Recommendations for design and construction of high performance fiber reinforced cement composites with multiple fine cracks (HPFRCC). Concr Eng Ser 2008;82. Testing Method 6-10, http://www.jsce.or.jp/committee/concrete/e/index.html.
[37] John Robert Prince M, Singh B. Bond behaviour of deformed steel bars embedded in recycled aggregate concrete. Constr Build Mater 2013;49:852–62. https://doi.org/10.1016/j.conbuildmat.2013.08.031.
[38] Alavi-Fard M, Marzouk H. Bond of high-strength concrete under monotonic pull-out loading. Mag Concr Res 2004;56:545–57. https://doi.org/10.1680/macr.56.9.545.53144.
[39] Lee SW, Kang SB, Tan KH, Yang EH. Experimental and analytical investigation on bond-slip behaviour of deformed bars embedded in engineered cementitious composites. Constr Build Mater 2016;127:494–503. https://doi.org/10.1016/j.conbuildmat.2016.10.036.
[40] Bheel N, Ali MOA, Kırgız MS, Shafiq N, Gobinath R. Effect of graphene oxide particle as nanomaterial in the production of engineered cementitious composites including superplasticizer, fly ash, and polyvinyl alcohol fiber. Mater Today Proc 2023. https://doi.org/10.1016/j.matpr.2023.03.010.
[41] Lv S, Ma Y, Qiu C, Sun T, Liu J, Zhou Q. Effect of graphene oxide nanosheets of microstructure and mechanical properties of cement composites. Constr Build Mater 2013;49:121–7. https://doi.org/10.1016/j.conbuildmat.2013.08.022.
[42] Zhao L, Guo X, Ge C, Li Q, Guo L, Shu X, Liu J. Mechanical behavior and toughening mechanism of polycarboxylate superplasticizer modified graphene oxide reinforced cement composites. Compos Part B Eng 2017;113:308–16. https://doi.org/10.1016/j.compositesb.2017.01.056.
[43] Yang H, Monasterio M, Cui H, Han N. Experimental study of the effects of graphene oxide on microstructure and properties of cement paste composite. Compos Part A Appl Sci Manuf 2017;102:263–72. https://doi.org/10.1016/j.compositesa.2017. 207.022.
[44] Lu Z, Hou D, Meng L, Sun G, Lu C, Li Z. Mechanism of cement paste reinforced by graphene oxide/carbon nanotubes composites with enhanced mechanical properties. RSC Adv 2015;5:100598–605. https://doi.org/10.1039/c5ra18602a.
[45] Shamsaei E, de Souza FB, Yao X, Benhelal E, Akbari A, Duan W. Graphene-based nanosheets for stronger and more durable concrete: a review. Constr Build Mater 2018;183:642–60. https://doi.org/10.1016/j.conbuildmat.2018.06.201.
[46] Liu J, Fu J, Yang Y, Gu C. Study on dispersion, mechanical and microstructure properties of cement paste incorporating graphene sheets. Constr Build Mater 2019;199:1–11. https://doi.org/10.1016/j.conbuildmat.2018.12.006.
[47] Young RJ, Liu M, Kinloch IA, Li S, Zhao X, Vallés C, Papageorgiou DG. The mechanics of reinforcement of polymers by graphene nanoplatelets. Compos Sci Technol 2018;154:110–6. https://doi.org/10.1016/j.compscitech.2017.11.007.
[48] Zhao L, Guo X, Song L, Song Y, Dai G, Liu J. An intensive review on the role of graphene oxide in cement-based materials. Constr Build Mater 2020;241. https://doi.org/10.1016/j.conbuildmat.2019.117939.
[49] Kang D, Seo KS, Lee HY, Chung W. Experimental study on mechanical strength of GO-cement composites. Constr Build Mater 2017;131:303–8. https://doi.org/10.1016/j.conbuildmat.2016.11.083.
[50] Mohammed A, Sanjayan JG, Duan WH, Nazari A. Incorporating graphene oxide in cement composites: a study of transport properties. Constr Build Mater 2015;84:341–7. https://doi.org/10.1016/j.conbuildmat.2015.01.083.
[51] Pan Z, He L, Qiu L, Korayem AH, Li G, Zhu JW, Collins F, Li D, Duan WH, Wang MC. Mechanical properties and microstructure of a graphene oxide-cement composite. Cem Concr Compos 2015;58:140–7. https://doi.org/10.1016/j.cemconcomp.2015.02.001.
[52] Gong K, Asce SM, Pan Z, Korayem AH, Ph D, Qiu L, Li D, Collins F, Wang CM, Duan WH, Asce a M. Reinforcing effects of graphene oxide on Portland cement paste. J Mater Civ Eng 2014;27:1–6.
[53] Lu C, Lu Z, Li Z, Leung CKY. Effect of graphene oxide on the mechanical behavior of strain hardening cementitious composites. Constr Build Mater 2016;120:457–64. https://doi.org/10.1016/j.conbuildmat.2016.05.122.

[54] Mokhtar MM, Abo-El-Enein SA, Hassaan MY, Morsy MS, Khalil MH. Mechanical performance, pore structure and micro-structural characteristics of graphene oxide nano platelets reinforced cement. Constr Build Mater 2017;138:333–9. https://doi.org/10.1016/j.conbuildmat.2017.02.021.
[55] Hou D, Lu Z, Li X, Ma H, Li Z. Reactive molecular dynamics and experimental study of graphene-cement composites: structure, dynamics and reinforcement mechanisms. Carbon N Y 2017;115:188–208. https://doi.org/10.1016/j.carbon.2017.01.013.
[56] M. Hou, K. Xu, P.J.M. Monteiro, V.C. Li, Rubber particle bridging effect on crack width control of low carbon Engineered Cementitious Composites (ECC), (n.d.).
[57] Zhang X, Nguyen H, Daly M, Nguyen SBT, Espinosa HD. Nanoscale toughening of ultrathin graphene oxide-polymer composites: mechanochemical insights into hydrogen-bonding/van der Waals interactions, polymer chain alignment, and steric parameters. Nanoscale 2019;11:12305–16. https://doi.org/10.1039/c9nr01453e.
[58] Sharma S, Rawal J, Dhakate SR, Singh BP. Synergistic bridging effects of graphene oxide and carbon nanotube on mechanical properties of aramid fiber reinforced polycarbonate composite tape. Compos Sci Technol 2020;199. https://doi.org/10.1016/j.compscitech.2020.108370.
[59] Amudha A, Shashikala HD, Asiq Rahman OS, Keshri AK, Nagaraja HS. Effect of graphene oxide loading on plasma sprayed alumina-graphene oxide composites for improved anticorrosive and hydrophobic surface. Surf Topogr Metrol Prop 2019;7. https://doi.org/10.1088/2051-672X/ab2707.
[60] Noushini A, Samali B, Vessalas K. Effect of polyvinyl alcohol (PVA) fibre on dynamic and material properties of fibre reinforced concrete. Constr Build Mater 2013;49:374–83. https://doi.org/10.1016/j.conbuildmat.2013.08.035.
[61] Mohammed BS, Achara BE, Nuruddin MF, Yaw M, Zulkefli MZ. Properties of nano-silica-modified self-compacting engineered cementitious composites. J Clean Prod 2017;162:1225–38. https://doi.org/10.1016/j.jclepro.2017.06.137.
[62] Yoo DY, Park JJ, Kim SW. Fiber pullout behavior of HPFRCC: effects of matrix strength and fiber type. Compos Struct 2017;174:263–76. https://doi.org/10.1016/j.compstruct.2017.04.064.
[63] Wang S, Li VC. Engineered cementitious composites with high-volume fly ash. ACI Mater J 2007;104:233–41. https://doi.org/10.14359/18668.
[64] Yeşilmen S, Al-Najjar Y, Balav MH, Şahmaran M, Yildirim G, Lachemi M. Nano-modification to improve the ductility of cementitious composites. Cement Concr Res 2015;76:170–9. https://doi.org/10.1016/j.cemconres.2015.05.026.
[65] Pop I, De Schutter G, Desnerck P, Onet T. Bond between powder type self-compacting concrete and steel reinforcement. Constr Build Mater 2013;41:824–33. https://doi.org/10.1016/j.conbuildmat.2012.12.029.
[66] ACI Committee 408. ACI 408R-03 bond and development of straight reinforcing bars in tension. 2003.
[67] Akcay B, Tasdemir MA. Optimisation of using lightweight aggregates in mitigating autogenous deformation of concrete. Constr Build Mater 2009;23:353–63. https://doi.org/10.1016/j.conbuildmat.2007.11.015.
[68] Khed VC, Mohammed BS, Shahir Liew M, Alaloul WS, Adamu M. Hybrid fibre rubberized ECC optimization for modulus of elasticity. Int J Civ Eng Technol 2018;9:918–28.
[69] Bayramov F, Taşdemir C, Taşdemir MA. Optimisation of steel fibre reinforced concretes by means of statistical response surface method. Cem Concr Compos 2004;26:665–75. https://doi.org/10.1016/S0958-9465(03)00161-6.
[70] Karihaloo BL, Lange-Kornbak D. Optimization techniques for the design of high-performance fibre-reinforced concrete. Struct Multidiscip Optim 2008;36:215. https://doi.org/10.1007/s00158-008-0275-y. 215.
[71] Grabiec AM, Piasta ZX. Study on compatibility of cement-superplasticiser assisted by multicriteria statistical optimisation. J Mater Process Technol 2004;152:197–203. https://doi.org/10.1016/j.jmatprotec.2004.03.020.
[72] Raamesh L, Uma GV. Data mining based optimization of test cases to enhance the reliability of the testing. Commun Comput Inf Sci 198 CCIS 2011:89–98. https://doi.org/10.1007/978-3-642-22555-0_10.
[73] Auta M, Hameed BH. Optimized waste tea activated carbon for adsorption of Methylene Blue and Acid Blue 29 dyes using response surface methodology. Chem Eng J 2011;175:233–43. https://doi.org/10.1016/j.cej.2011.09.100.
[74] Mohammed BS, Khed VC, Liew MS. Optimization of hybrid fibres in engineered cementitious composites. Constr Build Mater 2018;190:24–37. https://doi.org/10.1016/j.conbuildmat.2018.08.188.
[75] Ghafari E, Costa H, Júlio E. RSM-based model to predict the performance of self-compacting UHPC reinforced with hybrid steel micro-fibers. Constr Build Mater. 2014;66:375–83. https://doi.org/10.1016/j.conbuildmat.2014.05.064.
[76] Suich R, Derringer G. Simultaneous optimization of several response variables. J Qual Technol 1980;12:214–9.
[77] Wang X, Yu R, Shui Z, Song Q, Zhang Z. Mix design and characteristics evaluation of an eco-friendly Ultra-High Performance Concrete incorporating recycled coral based materials. J Clean Prod 2017;165:70–80. https://doi.org/10.1016/j.jclepro.2017.07.096.